Signaling from the RNA sensor RIG-I is regulated by ufmylation

Daltry L. Snider[1], Moonhee Park[1], Kristen A. Murphy[1], Dia C. Beachboard[1, a], Stacy M. Horner[1,2,*]

[1] Department of Molecular Genetics & Microbiology, Duke University Medical Center, Durham, NC 27710, USA

[2] Department of Medicine, Duke University Medical Center Durham, NC 27710, USA

[a] Current address: DeSales University, Center Valley, Pennsylvania, 18034

* Correspondence: stacy.horner@duke.edu
Stacy M. Horner, Ph.D.
Duke University Medical Center
213 Research Dr., Box 3053 DUMC
Durham, NC USA 27710

Keywords

Retinoic acid-inducible gene I, RLR signaling, ubiquitin-like modifications, mitochondrial-associated ER membranes

Abstract

The RNA binding protein RIG-I is a key initiator of the antiviral innate immune response. The signaling that mediates the antiviral response downstream of RIG-I is transduced through the adaptor protein MAVS and results in the induction of type I and III interferons (IFN). This signal transduction occurs at endoplasmic reticulum (ER)-mitochondrial contact sites, to which RIG-I and other signaling proteins are recruited following their activation. RIG-I signaling is highly regulated to prevent aberrant activation of this pathway and dysregulated induction of IFN. Previously, we identified UFL1, the E3 ligase of the ubiquitin-like modifier conjugation system called ufmylation, UFL1, as one of the proteins recruited to membranes at ER-mitochondrial contact sites in response to RIG-I activation. Here, we show that UFL1, as well as the process of ufmylation, promote IFN induction in response to RIG-I activation. We find that following RNA virus infection, UFL1 is recruited to the membrane targeting protein 14-3-3ε, and that this complex is then recruited to activated RIG-I to promote downstream innate immune signaling. Importantly, we found that 14-3-3ε has an increase in UFM1-conjugation following RIG-I activation. Additionally, loss of cellular ufmylation prevents the interaction of 14-3-3ε with RIG-I, which abrogates the interaction of RIG-I with MAVS and thus downstream signal transduction that induces IFN. Our results define ufmylation as an integral regulatory component of the RIG-I signaling pathway and as a post-translational control for IFN induction.

Significance

The viral RNA sensor RIG-I initiates the antiviral innate immune response by activating a signaling cascade that induces interferon. Activation of the RIG-I signaling pathway is highly regulated to quickly mount a protective immune response while preventing dysregulation that can lead to excessive inflammation or autoimmune disorders. Here, we characterize one such mechanism of regulation. We describe that UFL1, an E3 ligase for the ubiquitin-like modifier conjugation system called ufmylation, is important to promote RIG-I signaling. Using molecular approaches, we show that ufmylation promotes RIG-I interaction with the membrane targeting protein 14-3-3ε. As such, ufmylation positively regulates RIG-I recruitment to its signaling adaptor proteins MAVS for induction of interferon in response to RNA virus infection.

64 **Introduction**

65

66 Detection of RNA virus infection is initiated by cellular sensors such as RIG-I. RIG-I is a
67 pattern recognition receptor that detects unique features of viral RNA that are generally
68 absent in cellular RNA, referred to as pathogen-associated molecular patterns (PAMPs)
69 (1). Sensing of viral RNA PAMPs triggers RIG-I activation and induces a downstream
70 signaling cascade that ultimately results in transcriptional induction of type I and type III
71 interferons (IFN) and the antiviral response (2, 3). The RIG-I signaling cascade is carefully
72 regulated by multiple mechanisms, including post-translational modifications that
73 influence specific protein-protein interactions that can result in changes in protein
74 localization to mediated signaling (3, 4). For example, following sensing of RNA PAMPs,
75 RIG-I undergoes K63-linked polyubiquitination in order to transition to its fully active
76 conformation, which promotes its interaction with the molecular trafficking protein 14-3-3ε
77 (5–8). 14-3-3ε facilitates the recruitment of activated RIG-I from the cytosol to intracellular
78 membranes where it interacts with MAVS (7, 9, 10), which assembles other RIG-I pathway
79 members to transduce the signals that induce IFN (7, 11). Importantly, many RNA viruses,
80 including influenza A virus and some flaviviruses (dengue virus, Zika virus, and West Nile
81 virus), prevent the interaction of RIG-I with 14-3-3ε to limit IFN induction and evade the
82 antiviral response (9, 10, 12).

83

84 In addition to RIG-I, a number of signaling proteins must be recruited to MAVS in order to
85 propagate downstream IFN induction. Previously, we identified proteins that move to
86 MAVS signaling sites at mitochondrial-associated endoplasmic reticulum (ER)
87 membranes (MAM) during RNA virus infection (13, 14). These proteins likely aid in spatial
88 organization of RIG-I pathway proteins during viral infection and include the GTPase
89 RAB1B, which plays a role in recruiting TRAF3 to MAVS (15). In addition to RAB1B, we
90 identified other proteins recruited to the MAM upon RIG-I signaling activation, one of which
91 was UFL1 (referred to in our previous publication as KIAA0776) (14). UFL1 is an E3 ligase
92 for UFM1, which is a ubiquitin-like modification of 85 amino acids. The process of
93 ufmylation conjugates UFM1 covalently to lysine residues of target proteins through a
94 process called ufmylation, which is similar to ubiquitination in that it also uses an E1, E2,
95 and E3 ligase conjugation system (UBA5, UFC1, and UFL1; see Figure 2D). UFM1 is
96 removed by the UFSP2 protease (16–20). The consequence of UFM1 addition to proteins
97 is not fully understood, but the literature supports the idea that it can promote protein-

98 protein interactions to regulate a number of biological processes (21–31). Here, we
99 uncover a role for ufmylation in RIG-I activation. We found that the cellular proteins that
100 catalyze ufmylation all promote RIG-I-mediated induction of IFN. Interestingly, we found
101 that following RNA virus infection UFL1 interacts with both RIG-I and the molecular
102 trafficking protein 14-3-3ε, and that 14-3-3ε undergoes ufmylation. Further, similar to RIG-
103 I, UFL1 is recruited to intracellular membranes following RNA virus infection. Importantly,
104 loss of ufmylation prevents the interaction of 14-3-3ε with RIG-I, which results in
105 decreased MAVS activation and IFN induction in response to RNA virus infection. Thus,
106 ufmylation can regulate RIG-I activation and downstream signaling of the intracellular
107 innate immune system.
108
109 **Results**
110
111 **The ufmylation activity of UFL1 promotes RIG-I signaling.** Having found that the E3
112 ligase of ufmylation UFL1 is recruited to MAVS signaling sites at the MAM in response to
113 RIG-I signaling (14), we wanted to determine if UFL1 regulates RIG-I signaling. To test
114 this, we measured induction of the IFN-β promoter following UFL1 overexpression using
115 an IFN-β promoter luciferase reporter assay (32) and found that UFL1 increased activation
116 of the IFN-β promoter, similar to that of RIG-I expression, in a dose-dependent fashion in
117 response to infection with Sendai virus (SenV) (Figure 1A). SenV is a murine
118 paramyxovirus that specifically activates RIG-I (33). In support of UFL1 enhancing RIG-I
119 signaling specifically, exogenous expression of UFL1 also increased IFN-β promoter
120 activity in response to transfection of 293T cells with a known RIG-I immunostimulatory
121 RNA from hepatitis C virus (PAMP; Figure S1A) (34). However, UFL1 overexpression in
122 293T cells did not lead to increased induction of IFN-stimulated genes (ISG), such as
123 *ISG56* or *ISG15,* in response to exogenous IFN-β treatment, which bypasses RIG-I
124 signaling and IFN induction, indicating that UFL1 primarily regulates IFN induction and not
125 the IFN response (Figure S1B). Next, we depleted UFL1 by siRNA in two different cell
126 types and measured SenV-induced activation of the RIG-I pathway. Depletion of UFL1 in
127 primary neonatal human dermal fibroblasts (NHDFs) reduced the SenV-mediated
128 induction of both *IFNB1* and *IFNL1* transcripts, as measured by RT-qPCR (Figure 1B), as
129 well as production of IFN-β protein, as measured by an enzyme-linked immunosorbent
130 assay (ELISA) (Figure 1C). Depletion of UFL1 in 293T cells resulted in decreased
131 phosphorylation of IRF3, a transcription factor for both type I and III IFNs, while exogenous

132 expression of an siRNA-resistant UFL1 restored SenV-mediated IRF3 phosphorylation
133 (Figure 1D).
134
135 To define the domains of UFL1 that regulate RIG-I signaling, we expressed a series of
136 previously described UFL1 truncation mutants and measured SenV-mediated activation
137 of the IFN-β promoter in a luciferase reporter assay (16). The ability of UFL1 to transfer
138 UFM1 to a target protein has been suggested to require the first 212 amino acids of the
139 protein, as this domain interacts with the E2 ligase for ufmylation, UFC1 (16). The wild-
140 type (WT) UFL1 (aa 1-794), as well as the C-terminal deleted mutants of UFL1, aa 1-212
141 and aa 1-452, which all have reported ufmylation activity (16), stimulated SenV-medicated
142 induction of the IFN-β promoter (Figure 1E). Interestingly, the N-terminal deleted mutant
143 of UFL1 aa 213-794, which does not have reported ufmylation activity, also induced
144 signaling, while the N-terminal deleted UFL1 mutant aa 453-794 did not (Figure 1E). To
145 measure UFL1 conjugation activity in our hands, we quantified the formation of higher
146 molecular weight UFM1-conjugates by immunoblotting. The 10 kDa UFM1 protein is
147 known to be conjugated to a number of proteins, including the highly abundant RPL26 (21,
148 28). Indeed, our analysis of the higher molecular weight UFM1-conjugates induced by
149 these UFL1 constructs revealed differential abundance of these UFM1-conjugates.
150 Specifically, UFL1 WT, aa 1-212, aa 1-452, and aa 213-794 of UFL1 all retain full
151 ufmylation activity, while aa 453-794 of UFL1 does not (Figure S1C). Thus, taken together,
152 this reveals that the ufmylation activity of UFL1 is required to promote RIG-I signaling that
153 results in induction of IFN.
154
155 **The ufmylation machinery proteins positively regulate RIG-I signaling.** Having
156 determined that the ufmylation activity of UFL1 is important for its role in RIG-I signaling,
157 we hypothesized that UFM1 and the proteins required for UFM1 conjugation would also
158 be required to promote this signaling. Similar to our results with UFL1, overexpression of
159 UFM1 increased SenV-mediated activation of the IFN-β promoter, resembling the
160 magnitude of induction seen with RIG-I, in a dose-dependent fashion (Figure 2A).
161 Conversely, the activation of the IFN-β promoter in response to SenV was significantly
162 abrogated in 293T cells in which UFM1 was deleted by CRISPR/Cas9, as compared to
163 WT 293T cells (Figure 2B). Importantly, this signaling was restored upon exogenous
164 expression of UFM1 (Figure 2B). The absence of UFM1 expression also prevented the
165 induction of IFN-β protein in response to SenV infection, as measured by ELISA (Figure

166 2C). The process of ufmylation has 5 steps (Figure 2D). First, UFM1 is processed to
167 expose the terminal glycine residue. Then, this mature UFM1 is added to the target protein
168 by the actions of UBA5, which acts as an E1 ligase for UFM1; UFC1, the E2 ligase; and
169 UFL1, the E3 ligase (19). Finally, the UFSP2 protease removes UFM1, which enables
170 recycling of mature UFM1 (18). We found that exogenous expression of each of the
171 proteins involved in UFM1 conjugation, including the UFSP2 protease, positively regulated
172 SenV-mediated induction of the IFN-β promoter (Figure 2E). Conversely, the induction of
173 *IFNB1* by SenV was abrogated in 293T cells in which UFSP2 was deleted by
174 CRISPR/Cas9, similar to that seen upon UFM1 KO. Interestingly, we observed an
175 increase in UFM1-retention by an ufmylated protein and a decrease in free UFM1 in the
176 UFSP2 KO cells via anti-UFM1 immunoblot, suggesting UFSP2 may serve to primarily to
177 increase the pool of available mature UFM1 for conjugation (Figure 2F). These results
178 reveal that the proteins that catalyze ufmylation and the UFM1 modification itself promote
179 RIG-I signaling.
180
181 **UFM1 is required for the RIG-I-driven transcriptional response.** After establishing that
182 ufmylation promotes RIG-I activation, and in turn IFN expression, we next broadly
183 measured the impact of ufmylation upon the transcriptional response to RIG-I signaling.
184 Using RNA-sequencing, we analyzed gene expression in either WT or UFM1 KO 293T
185 cells, following mock or SenV infection (Table S1.1; Table S1.2). Gene set enrichment
186 analysis (Table S2.1; Table S2.2) of the transcripts significantly reduced (adjusted $P<0.01$)
187 by UFM1 KO in the absence of viral infection revealed previously described pathways
188 regulated by ufmylation such as cytosolic ribosomes, ribosome assembly, and
189 hematopoiesis (Figure S2A; Table S2.1) (21, 28, 29, 35). Following viral infection, the top
190 10 gene categories negatively impacted by UFM1 KO, with a darker red color indicating
191 more downregulation, were all related to the antiviral response, such as response to type
192 I IFN and defense against virus (Figure 3A; Table S2.2). Indeed, of the top 50 most
193 downregulated pathways impacted by UFM1 KO during infection, the majority were related
194 to innate immune signaling or viral replication (Table S2.2), while upregulated gene
195 categories were more diverse (Table S2.3; Table S2.4). Of the genes differentially
196 expressed during UFM1 KO in response to SenV (adjusted $P<0.01$), the majority are
197 downregulated (Figure 3B). Indeed, these downregulated genes included *IFNB1* and
198 *IFNL1*, as well as other known ISGs (in red) (36) (Figure 3B; Figure 3C). These data are

199 consistent with a model in which ufmylation-mediated regulation of IFN induction has
200 broad consequences on genes induced by the IFN response.
201
202 **UFL1 is recruited to intracellular membranes and interacts with 14-3-3ε and RIG-I**
203 **during RNA virus infection.** Following the binding of RIG-I to non-self RNA, it interacts
204 with several host proteins to facilitate its activation, localization to the MAM, and interaction
205 with MAVS. These proteins include the E3 ligases for K63-linked ubiquitin Riplet and
206 TRIM25 (5, 6, 37), as well as the molecular trafficking protein 14-3-3ε. In particular, 14-3-
207 3ε is required for RIG-I recruitment from the cytosol to MAVS signaling sites at intracellular
208 membranes (5–7, 13); however, the mechanism underlying how 14-3-3ε selects RIG-I as
209 cargo has yet to be elucidated. Using a subcellular membrane fractionation assay (38),
210 we confirmed that UFL1 increases its association with intracellular membranes in
211 response to SenV, similar to RIG-I (Figure 4A; compare fraction #1, which has Cox-I and
212 no GAPDH, with fractions #6-8, which are enriched for the cytosolic protein GAPDH) (7,
213 12). This finding is consistent with our previous report that UFL1 is recruited to the MAM
214 in response to either SenV or hepatitis C virus replication (14), suggesting that UFL1
215 recruitment occurs prior to MAVS activation, as MAVS is cleaved by the HCV NS3-NS4A
216 protease (39–42). As the recruitment of RIG-I to intracellular membranes is known to
217 require 14-3-3ε, and, as both UFL1 and UFM1 have been shown to interact with 14-3-3ε
218 (16), we hypothesized that UFL1 may interact with 14-3-3ε to promote the IFN induction
219 that we had observed in response to RNA virus infection. Thus, we first determined if the
220 interaction of UFL1 with 14-3-3ε is increased in response to RIG-I activation by SenV by
221 performing co-immunoprecipitation. We found that Myc-14-3-3ε did co-immunoprecipitate
222 with Flag-UFL1, as reported previously (16), and that this interaction was increased by
223 SenV (Figure 4B). Interestingly, the interaction of UFL1 with RIG-I also increased following
224 SenV, both upon over-expression and at the level of the endogenous proteins (Figure 4C;
225 Figure 4D). As RIG-I undergoes a series of modifications to become fully active (1, 4), we
226 next used a panel of RIG-I mutants to define which stage of RIG-I activation promotes
227 interaction with UFL1. These mutations prevent the distinct steps of RIG-I activation such
228 as RIG-I binding to RNA (K888/907A), interacting with TRIM25 (T55I), or ubiquitination by
229 Riplet and TRIM25 (K172/788R) (5, 43, 44). The interaction of UFL1 with RIG-I was
230 significantly impaired by each of these mutations, suggesting that UFL1 regulates RIG-I
231 function after it binds RNA and becomes ubiquitinated (Figure 4E). As this is the same

232 step of activation at which 14-3-3ε binds to RIG-I to promote its translocation to
233 intracellular membranes (7), we next tested the ability of UFL1 to promote RIG-I signaling
234 in conjunction with the RIG-I regulatory factors Riplet and 14-3-3ε (6, 7). We found that
235 co-expression of equal amounts of UFL1 with either Riplet or 14-3-3ε increased SenV-
236 mediated activation of the IFN-β promoter above that seen by the individual proteins
237 (Figure 4F). Intriguingly, the expression of UFL1 appears to be stabilized or enhances in
238 the presence of Riplet and 14-3-3ε. These data together suggest that RNA virus infection
239 increases the interaction of 14-3-3ε with UFL1, which then interacts with activated, K63-
240 ubiquitinated RIG-I to promote downstream signaling.
241
242 **UFL1 interaction with RIG-I requires 14-3-3ε and UFM1.** Having determined that UFL1
243 interacts with both activated RIG-I and 14-3-3ε following RNA virus infection, we next
244 defined the dynamics of this complex formation by testing two distinct models. In the first
245 model, UFL1 would interact first with activated RIG-I, induce its ufmylation, and then the
246 UFL1-RIG-I complex would interact with 14-3-3ε. In this model, depletion of 14-3-3ε or
247 loss of UFM1 would not be expected to change the interaction of UFL1 with RIG-I. In the
248 second model, UFL1 would interact first with 14-3-3ε and induces its ufmylation, or that of
249 another associated protein, and then the UFL1-14-3-3ε complex would interact with
250 activated RIG-I. In this second model, depletion of 14-3-3ε would be expected to prevent
251 UFL1 interaction with RIG-I, and loss of ufmylation would limit UFL1 interaction with RIG-
252 I but would not affect UFL1 interaction with 14-3-3ε. To elucidate these possibilities, first,
253 we used co-immunoprecipitation to measure the interaction of exogenously expressed
254 Flag-UFL1 and HA-RIG-I in SenV-infected 293T lysates that had been depleted of 14-3-
255 3ε or CTRL by siRNA. This revealed that formation of the SenV-activated RIG-I-UFL1
256 complex requires 14-3-3ε (Figure 5A). Next, we tested if ufmylation was required for
257 formation of the SenV-activated RIG-I-UFL1 complex by measuring this interaction in WT
258 or UFM1 KO 293T cells. We found that UFM1 was required for SenV-activated RIG-I-
259 UFL1 complex (Figure 5B). The results of these two experiments reveal that both 14-3-3ε
260 and UFM1 are required for UFL1 to interact with RIG-I, supporting the second model of
261 complex formation in which UFL1 interacts first with 14-3-3ε and catalyzes its ufmylation,
262 and then this complex associates with RIG-I. In support of this, we found that UFM1 was
263 not required for UFL1 to interact with 14-3-3ε (Figure 5C). To test if 14-3-3ε is UFM1-
264 conjugated , we performed an immunoprecipitation of Flag-14-3-3ε from cell extracts that

265 were mock or SenV-infected and expressed either HA-UFM1-WT or HA-UFM1DC3, which
266 lacks the terminal 3 amino acids required conjugation to target proteins (17). Importantly,
267 these extracts were boiled prior to immunoprecipitation to remove non-covalent
268 interactions. Following immunoprecipitation of Flag-14-3-3ε, immunoblotting with an anti-
269 HA antibody revealed a slower migrating form of 14-3-3ε approximately 15 kDa heavier
270 (HA+UFM1) than the predicted molecular weight of 14-3-3ε (37 kDa) (Figure 5D),
271 suggestive of covalent UFM1 modification. Additionally, the proportion of 14-3-3ε,
272 conjugated by UFM1 increases following SenV infection. Together, these data indicate
273 that ufmylation promotes the interaction of UFL1 with 14-3-3ε and activated RIG-I and that
274 UFM1 has increased conjugation to 14-3-3ε following RIG-I activation.
275
276 **Ufmylation promotes RIG-I interaction with 14-3-3ε for MAVS activation.** Having
277 found that that UFL1 requires 14-3-3ε to interact with activated RIG-I, we next tested if
278 UFL1 is required for the interaction of 14-3-3ε with RIG-I, which is essential for activated
279 RIG-I to translocate from the cytosol to intracellular membranes for interaction with MAVS
280 (7). We performed a co-immunoprecipitation of Flag-RIG-I and Myc-14-3-3ε from 293T
281 cells and found that this SenV-mediated interaction was significantly decreased upon
282 UFL1 depletion (Figure 6A). In addition, loss of UFM1 expression also decreased the
283 SenV-induced interaction of RIG-I with 14-3-3ε (Figure S3). Importantly, we also found
284 that UFM1 is required for the SenV-induced interaction of RIG-I with MAVS (Figure 6B)
285 and MAVS higher-order oligomerization, which is a hallmark of MAVS activation (45, 46)
286 (Figure 6C). In summary, these data reveal that UFL1 and UFM1 are required for the RIG-
287 I interaction with 14-3-3ε, for interaction with MAVS, and for MAVS activation by
288 oligomerization.
289
290 **Discussion**
291
292 Regulation of RIG-I activation and downstream signaling is essential for proper induction
293 and termination of IFN. Here, we show that both UFL1 and the process of ufmylation
294 promote RIG-I pathway signaling that leads to IFN induction, uncovering an important step
295 in the activation of the RIG-I pathway. RIG-I activation occurs upon RNA binding. Then,
296 RIG-I undergoes ATP hydrolysis. And interaction with K63-linked polyubiquitin chains,
297 both covalently and non-covalently (5, 44, 47), which promotes formation of a RIG-I

298 tetramer (48). This polyubiquitinated, activated RIG-I oligomer then interacts with the
299 membrane trafficking protein 14-3-3ε for translocation to MAVS at ER-mitochondrial
300 contact sites (7). We found that UFL1 is recruited to 14-3-3ε following RNA virus infection
301 and that ufmylation facilitates the interaction between 14-3-3ε and activated RIG-I.
302 Importantly, this results in increased interaction of RIG-I with MAVS and MAVS
303 oligomerization, ultimately promoting the downstream signal transduction which produces
304 IFN.
305
306 Ufmylation is emerging as a post-translational modification that regulates diverse
307 biological processes, including DNA repair, ER homeostasis, and even the replication of
308 hepatitis A virus (21, 22, 24, 27, 28, 30, 35, 49). In these cases, UFL1, along with the other
309 members of the ufmylation cascade, induce ufmylation of a target protein important for
310 regulating these processes. For example, both MRE11 and histone H4 are ufmylated by
311 UFL1 in the nucleus in response to DNA damage resulting in activation the key DNA repair
312 kinase ATM (22, 24). UFL1 can also act at the ER, where it plays a role in ER protein
313 quality control, where it ufmylates specific proteins, including ribosomal proteins RPL26,
314 to induce lysosomal degradation of stalled peptides and/or the ER and prevent the
315 unfolded protein response (27, 28, 49, 50). Hepatitis A virus translation, which occurs in
316 association with the ER, also requires ufmylation of RPL26 (30). Therefore, ufmylation can
317 regulate several aspects of translation. It is possible that ufmylation regulates translation
318 of certain mRNAs important for RIG-I signaling and subsequent IFN induction. However,
319 we identified a role for ufmylation in regulating the interaction of RIG-I with 14-3-3ε, one
320 of the earliest known steps of RIG-I signaling, strongly supporting a mechanism in which
321 following RIG-I activation, ufmylation is controlling this specific protein-protein interaction.
322 The mechanisms by which the process of UFM1 addition regulates interactions between
323 proteins or alters other aspects of protein function are largely unknown. Indeed, we found
324 that in both overexpression and KO conditions UFSP2, the protease that removes UFM1
325 from proteins (Figure 2D) (18), also promoted SenV-mediated IFN induction (Figure 2E-
326 F), suggesting that we do not yet have a full grasp on the ufmylation process. It is possible
327 that the dynamic process of ufmylation or the enhanced formation of mature UFM1
328 following deconjugation from targets promote RIG-I signaling independent of
329 deconjugation activity. Interestingly, in the UFSP2 KO cells, we observed increased
330 amounts of a specific higher molecular weight UFM1-conjugates by immunoblot,
331 suggesting that UFSP2 is important for the generation of free UFM1 for conjugation

332 (Figure 2F). Indeed, in support of this idea, others have shown that UFSP2 in myeloid
333 cells is required for influenza virus resistance in mice (31). It is also possible that UFSP2
334 acts on other members of the RIG-I pathway to alter their function. Future studies to define
335 how the process of ufmylation regulates this and other aspects of the antiviral innate
336 immune response will be of great interest as they may shed light broadly on how
337 ufmylation regulates diverse cell biological processes that alter cellular signaling.
338
339 The mechanisms underlying how cytoplasmic UFL1 is recruited to its protein targets that
340 reside in different subcellular compartments are not fully known. For example, we found
341 that RIG-I activation induces UFL1 translocation to intracellular membranes (Figure 3A),
342 and while we know that UFL1 is recruited to the MAM during infection, the mechanism by
343 which UFL1 becomes membrane-associated remains unknown (14). DDRGK1 (UFBP1)
344 may facilitate UFL1 targeting to the MAM, as DDRGK1 is localized to mitochondrial-ER
345 contact sites (16, 51) and in some cases it is required for UFL1 recruitment to membranes
346 (27, 28). Thus, both DDRGK1 and mitochondrial-ER contact sites could function as a
347 regulatory hub that aids in the recruitment of UFL1 and RIG-I pathway signaling proteins.
348 Interestingly, RAB1B, a GTPase that we found is recruited to the MAM and important for
349 RIG-I signaling (14, 15) is ufmylated (52, 53), which reveals that ufmylation likely regulates
350 a number of RIG-I pathway signaling proteins. As UFL1 contains no functional domains
351 common to other E3 ligases that might allow one to predict how its targets are selected
352 (16, 54, 55), defining the signals and features that control UFL1 localization, as well as
353 the target proteins ufmylated in response to RIG-I activation, will undoubtedly reveal clues
354 into how the process of ufmylation is activated and how specific targets are selected.
355
356 Our work revealed that 14-3-3ε required ufmylation to interact with activated RIG-I. The
357 details underlying how 14-3-3ε interacts with activated RIG-I have not been fully
358 elucidated, as it does not occur through the known phosphorylated amino acids on RIG-I,
359 the typical recruitment signal of the 14-3-3 family of proteins (7, 56, 57). Our work supports
360 the work of others demonstrating that 14-3-3ε interacts with UFM1 and other members of
361 the ufmylation pathway, and it reveals that SenV increases the proportion of ufmylated 14-
362 3-3ε (Figure 5D) (16). It is likely that 14-3-3ε is mono-ufmylated as the apparent molecular
363 weight of 14-3-3ε increased by one ufmylation group (HA+UFM1, 15 kDa; Figure 5D).
364 Thus, taken together with our results, this suggests that ufmylation of 14-3-3ε or a 14-3-
365 3ε-associated protein promotes the interaction between activated RIG-I and 14-3-3ε. In

366 fact, a number of 14-3-3 family proteins are post-translationally modified by
367 phosphorylation, acetylation, and oxidation (58). Therefore, post-translational modification
368 of 14-3-3ε by ufmylation could define how cargo proteins, including RIG-I, are selected.
369 Indeed, this mechanism could be shared with other RNA virus sensing pathways, such as
370 the RIG-I-like-receptor MDA5, which also interacts with a 14-3-3 protein, 14-3-3η, by an
371 unknown mechanism (59). Thus, ufmylation may broadly influence how 14-3-3 proteins or
372 other host proteins interact with each other to regulate the intracellular innate immune
373 response.
374
375 Overall, this work lays the groundwork for future studies to define how ufmylation of
376 antiviral innate immune signaling proteins regulates their function and how specific
377 signaling pathways are differentially activated through ufmylation. In addition, our work
378 adds ufmylation to the growing list of ubiquitin-like and other modifications that regulate
379 the intracellular innate immune response, including ISGylation, SUMOylation, FATylation,
380 acetylation, phosphorylation, and others (4, 60, 61) broadening our understanding of how
381 RIG-I signaling is activated and rapidly controlled by post-translational modifications in
382 response to infection, leading to greater knowledge of the exquisite regulation of these
383 pathways.
384
385 **Materials and Methods**
386
387 **Cell lines, viruses, and treatments.** Neonatal human dermal fibroblast (NHDF) cells and
388 embryonic kidney 293T cells were grown in Dulbecco's modification of Eagle's medium
389 (DMEM; Mediatech) supplemented with 10% fetal bovine serum (Thermo Fisher
390 Scientific), 1X minimum essential medium non-essential amino acids (Thermo Fisher
391 Scientific), and 25 mM HEPES (Thermo Fisher Scientific) (cDMEM). 293T (CRL-3216)
392 were obtained from American Type Culture Collection (ATCC), NHDF cells (CC-2509)
393 were obtained from Lonza. All cell lines were verified as mycoplasma free by the LookOut
394 Mycoplasma PCR detection kit (Sigma). SenV Cantell strain was obtained from Charles
395 River Laboratories and used at 200 hemagglutination units/mL (HAU). SenV infections
396 were performed in serum-free media (30 minutes to 1 hour), after which complete media
397 was replenished. IFN-β (PBL Assay Science) was added to cells at a concentration of 50
398 units/mL in cDMEM for 18 hours.
399

400 **Plasmids.** The following plasmids have been previously described: pEF-TAK-Flag, pEF-
401 BOS-Flag-RIG-I (62), pEF-TAK-Flag-Riplet (63) pIFN-β-luc (64), pCMV-Renilla
402 (Promega), pX459 (Addgene #62988), psPAX2 (Addgene #12260), and pMD2.G
403 (Addgene #12259), pEF-BOS-Flag-RIG-I T55I (65), pEF-TAK-Myc-MAVS (32).
404 pLJM1_Flag-UFM1 was a gift from Drs. Craig McCormick and John Rohde at Dalhouise
405 University. The following plasmids were generated by insertion of PCR-amplified
406 fragments into the NotI-to-PmeI digested pEF-TAK-Flag using InFusion cloning
407 (Clontech): pEF-TAK-Flag-UFL1 (GenBank: BC036379; GeneID: 23376), pEF-TAK-Flag-
408 UBA5 (NM_024818.6), pEF-TAK-Flag-UFC1 (NM_016406.4), pEF-TAK-Flag-UFSP2
409 (NM_018359.5), pEF-TAK-Flag-UFL1 1-212, pEF-TAK-Flag-UFL1 1-452, pEF-TAK-Flag-
410 UFL1 213-794, pEF-TAK-Flag-UFL1 453-794, and pEF-TAK-Flag-14-3-3ε. Both pEF-
411 TAK-Myc-14-3-3e and pEF-TAK-Myc-UFL1 were generated by insertion of PCR-amplified
412 fragments into the AgeI-NotI digested pEF-TAK-Myc (pEF-TAK-Myc-MAVS) by InFusion.
413 The pEF-TAK-HA vector was generated by PCR to replace Flag with HA, and pEF-TAK-
414 HA-RIG-I, and pEF-TAK-HA-UFM1 were generated by insertion of a PCR-amplified
415 fragment into the NotI-AgeI digested pEF-TAK-HA vector. pLEX-Flag-14-3-3e was
416 generated by ligation of a PCR-amplified Flag-14-3-3e into the BamHI-to-XhoI digested
417 pLEX using InFusion cloning. The following plasmids were generated by site-directed
418 mutagenesis: pEF-TAK-Flag-UFL1^{siR}, pEF-TAK-HA-UFM1DC3, pEF-BOS-Flag-RIG-I
419 K888/907A, and pEF-BOS-Flag-RIG-I K172/788R. To generate the CRISPR guide RNA
420 plasmids px459-UFM1-E2, px459-UFM1-B, and px459-UFSP2 sgRNA oligonucleotides
421 were annealed and inserted into the BbsI-digested pX459 (30, 66). The plasmid
422 sequences were verified by DNA sequencing and oligonucleotide sequences are available
423 upon request.
424
425 **Generation of RNA PAMP.** Annealed oligonucleotides containing the sequence of the
426 HCV 5'ppp poly-U/UC region (34) were *in vitro* transcribed using the MEGAshortscript T7
427 transcription kit (Ambion) followed by ethanol precipitation, with the resulting RNA
428 resuspended at 1 µg/µL.
429
430 **Transfection.** DNA transfections were performed using FuGENE6 (Promega) or TransIT-
431 LT1 (Mirus Bio). RNA PAMP transfections were done using the TransIT-mRNA
432 Transfection kit (Mirus Bio). The siRNA transfections were done using Lipofectamine
433 RNAiMax (Invitrogen). siRNAs directed against 14-3-3ε (Dharmacon-L-017302-02-0005),

434 UFL1 (Qiagen-SI04371318) or non-targeting AllStars negative control siRNA (Qiagen-
435 1027280) were transfected into 293T cells (25 pmol of siRNA; final concentration of 0.0125
436 μM) or NHDF cells (250 pmol of siRNA; final concentration of 0.25 μM). Media was
437 changed 4-24 hours post-transfection, and cells were incubated for 36-48 h post-
438 transfection prior to each experimental treatment. IFN-β-promoter luciferase assays were
439 performed as previously described at 18-24 hours post treatment and normalized to the
440 *Renilla* luciferase transfection control (33).
441
442 **ELISA.** IFN-β ELISAs were performed using Human IFN-beta DuoSet (R&D Systems)
443 with supernatants collected from cultured cells.
444
445 **Generation of cell lines**. UFM1 and UFSP2 KO 293T cells were generated by
446 CRISPR/Cas9, using two guides targeting exon 2 and 3 (UFM1) or a single guide targeting
447 exon 6 (UFSP2), similar to others, as we have done previously. Single cell clones were
448 validated via anti-UFM1 or anti-UFSP2 immunoblot and genomic sequencing, with one
449 clone used here (15, 30). 293T cell pools overexpressing Flag-14-3-3e were generated
450 by lentiviral transduction, as previously (36).
451
452 **RNA analysis.** Total cellular RNA was extracted using the RNeasy Plus mini kit (Qiagen).
453 RNA was then reverse transcribed using the iScript cDNA synthesis kit (BioRad), as per
454 the manufacturer's instructions. The resulting cDNA was diluted 1:3 in ddH2O. RT-qPCR
455 was performed in triplicate using the Power SYBR Green PCR master mix (Thermo-
456 Fisher) and QuantStudio 6 Flex RT-PCR system. Oligonucleotide sequences for qPCR
457 are available upon request.
458
459 **RNA-seq.** WT and UFM1 KO 293T cells were mock or SenV-infected (18 h) and
460 harvested in biological duplicate, followed by total RNA extraction via TRIzol reagent
461 (Thermo Fisher Scientific). Sequencing libraries were prepared using the KAPA Stranded
462 mRNA-Seq Kit (Roche) and sequenced on an Illumina Novaseq 6000 with 50 bp paired-
463 end reads (>20 million reads per sample) in an S1 flow cell by the Duke University Center
464 for Genomic and Computational Biology. RNA-seq data was processed using the
465 TrimGalore toolkit (67) which employs Cutadapt (68) to trim low-quality bases and Illumina
466 sequencing adapters from the 3' end of the reads. Only reads that were 20nt or longer
467 after trimming were kept for further analysis. Reads were mapped to the GRCh38v93

468 version of the human genome and transcriptome (69) using the STAR RNA-seq alignment
469 tool (70). Reads were kept for subsequent analysis if they mapped to a single genomic
470 location. Gene counts were compiled using the HTSeq tool (71). Only genes that had at
471 least 10 reads in any given library were used in subsequent analysis. Normalization and
472 differential expression was carried out using the DESeq2 (72) Bioconductor (73) package
473 with the R statistical programming environment. The false discovery rate was calculated
474 to control for multiple hypothesis testing. Gene set enrichment analysis (74) was
475 performed to identify gene ontology terms and pathways associated with altered gene
476 expression for each of the comparisons performed. All RNA-seq data are deposited in the
477 GEO database under GSE186287.
478
479 **Immunoblotting.** Cells were lysed in a modified radioimmunoprecipitation assay (RIPA)
480 buffer (10 mM Tris [pH 7.5], 150 mM NaCl, 0.5% sodium deoxycholate, and 1% Triton X-
481 100) supplemented with protease inhibitor cocktail (Sigma) and Halt Phosphatase Inhibitor
482 (Thermo-Fisher), and post-nuclear lysates were isolated by centrifugation. Quantified
483 protein (between 5 -15 µg) was resolved by SDS/PAGE, transferred to nitrocellulose or
484 polyvinylidene difluoride (PVDF) membranes in a 25 mM Tris-192 mM glycine-0.01% SDS
485 buffer. Membranes were stained with Revert 700 total protein stain (LI-COR Biosciences)
486 and then blocked in 3% BSA in Tris-buffered saline containing 0.01% Tween-20 (TBS-T).
487 After washing with PBS-T or TBS-T (for phosphoproteins) buffer, following incubation with
488 primary antibodies, membranes were incubated with species-specific horseradish
489 peroxidase-conjugated antibodies (Jackson ImmunoResearch, 1:5000) or fluorescent
490 secondaries (LI-COR Biosciences), followed by treatment of the membrane with Clarity
491 Western ECL substrate (BioRad) and imaging on a LICOR Odyssey FC. The following
492 antibodies were used for immunoblotting: R-anti-SenV (MBL, 1:1000), M-anti-Tubulin
493 (Sigma, 1:1000), R-anti-GAPDH (Cell Signaling Technology, 1:1000), R-anti-p-IRF3 (Cell
494 Signaling Technology, 1:1000), R-anti-IRF3 (Cell Signaling Technology, 1:1000), R-anti-
495 UFL1 (Novus Biologicals, 1:1000), R-anti-UFM1 (Abcam, 1:1000), anti-RIG-I (M-
496 AdipoGen, R-Abcam, 1:1000), R-anti-14-3-3ε (Cell Signaling Technology, 1:1000), M-anti-
497 Flag M2 (Sigma, 1:1000), anti-Flag-HRP (Sigma, 1:1000-1:5000), R-anti-Flag (Sigma,
498 1:1000), anti-HA (M- and R-Sigma, 1:1000), and anti-Myc (M-Santa Cruz or R-Cell
499 Signaling Technology, 1:1000).
500

501 **Immunoprecipitation.** Cells were lysed in RIPA buffer with or without 10% glycerol.
502 Quantified protein (between 100-500 µg) was incubated with protein-specific, isotype
503 control antibody (R-Cell Signaling Technology or M-Thermo Fisher), or anti-Flag M2
504 magnetic beads (Sigma), in lysis buffer either at room temperature for 2 h or at 4ºC
505 overnight with head over tail rotation. The lysate/antibody mixture was then incubated with
506 Protein G Dynabeads (Invitrogen) for 1 h. Beads were washed 3X in PBS or RIPA buffer
507 and eluted in 2X Laemmli Buffer (BioRad) with or without 5% 2-Mercaptoethanol at 95ºC
508 for 5 min. Proteins were resolved by SDS/PAGE and immunoblotting, as above. For
509 ufmylation immunoprecipitations, cells were lysed with NP-40 buffer (50 mM Tris [pH 8],
510 150 mM NaCl, 0.5% sodium deoxycholate, and 1% NP-40) supplemented with 10%
511 glycerol, protease and phosphatase inhibitors, as above, and N-ethylmaleimide (Sigma-
512 Aldrich). Post-nuclear lysates were boiled at 95°C for 5 min and incubated with anti-Flag
513 M2 magnetic beads, as above.
514
515 **Subcellular membrane fractionation.** Membrane fractionation was performed as
516 previously described (7, 12, 38, 75). Cells were lysed in hypotonic buffer (10 mM Tris-HCL
517 (pH 7.5), 10 mM KCl, and 5 mM $MgCl_2$ supplemented with protease inhibitor cocktail) for
518 10 minutes on ice followed by 20 passages through a 20-guage needle. Nuclei and
519 unbroken cells were removed by centrifugation at 1000xg for 5 min at 4ºC. The resulting
520 supernatants were mixed thoroughly with 72% sucrose and overlayed with 55% sucrose,
521 followed by 10% sucrose, all in low-salt buffer (2 nM EDTA, 20 nM HEPES (pH 8.0), 150
522 mM NaCl, 0.1% SDS, 1% Triton X-100). The gradients were subjected to centrifugation at
523 38,000 RPM in a Beckman SW41 Ti Rotor for 14 h at 4ºC. 1 mL fractions were collected
524 using a BioComp piston gradient fractionator and resulting fractions were divided in half
525 and mixed with 2 parts 100% methanol and precipitated overnight at -80ºC. Protein pellets
526 were collected by centrifugation and resuspended in 2X Laemmli buffer and heated for 5
527 min at 95ºC for immunoblot analysis. 10% pre-fractionated cells from each condition were
528 collected as the input.
529
530 **Semi-denaturing detergent agarose gel electrophoresis.** SDD-AGE was performed as
531 described (45, 46). Briefly, crude mitochondria (P5 fraction) were isolated from an equal
532 number of WT or UFM1 KO 293T cells that were mock or SenV infected (12 h),
533 resuspended in hypotonic buffer (10 mM Tris, pH 7.5, 10 mM KCl, 1.5 mM $MgCl_2$, and 0.5
534 mM EDTA). Resulting samples were split and 2X SDD-AGE sample buffer (0.5X TBE,

535 10% glycerol, 2% SDS, 0.2 mM Bromophenol Blue) buffer with or without 5% 2-
536 Mercaptoethanol was added, and samples were loaded onto a vertical 1.5% agarose gel.
537 Electrophoresis was performed with a constant voltage of 70 V at 4 °C in SDD-AGE
538 running buffer (1X TBE and 0.1% SDS). Gels were transferred onto a nitrocellulose
539 membrane overnight on ice at 25 V. Membranes were fixed in 0.25% glutaraldehyde in
540 PBS and immunoblotting was performed as usual. 15% of the SDD-AGE samples were
541 reserved for input.
542
543 **Quantification of immunoblots.** Immunoblots imaged using the LICOR Odyssey FC
544 were quantified by ImageStudio software, and raw values were normalized to relevant
545 controls for each antibody. Phosphoprotein values were normalized to Tubulin and
546 displayed as the percentage of signal from WT. Relative membrane association of UFL1
547 was quantified as the ratio of UFL1 to Cox-1 in fraction 1 normalized to total protein levels
548 of UFL1 in the input and displayed as the percentage of UFL1 membrane association
549 normalized to mock values.
550
551 **Statistical analysis.** Student's unpaired t-test, one-way ANOVA, or two-way ANOVA
552 were implemented for statistical analysis of the data followed by appropriate post-hoc test
553 (as indicated) using GraphPad Prism software. Graphed values are presented as mean ±
554 SD or SEM (n = 3 or as indicated); *$p \leq 0.05$, **$p \leq 0.01$, and ***$p \leq 0.001$.
555
556 **Acknowledgments**
557
558 We thank colleagues who provided reagents (see Methods), the Duke Functional
559 Genomics Core Facility, the Duke University Center for Genomic and Computational
560 Biology, the Duke Genomic Analysis and Bioinformatics Shared Resource and Dr. Wei
561 Chen for performing RNA-seq analysis, Dr. Madhuvanthi Vijayan and Boyoung Michelle
562 Kim for generation and initial characterization of plasmids, Dr. Matthew Thompson for
563 input in RNA-seq sample preparation and data processing, and Horner lab members for
564 useful discussion. This work was supported by funds from Burroughs Wellcome Fund,
565 National Institutes of Health: R21AI144380, R01AI155512, T32-CA009111, and an
566 American Cancer Society Postdoctoral fellowship 131321-PF-17-188-01-MPC.
567

Author Contributions: Conceptualization: D.L.S., D.C.B., and S.M.H.; Investigation: D.L.S, D.C.B., and M.P.; Formal analysis: D.L.S., D.C.B., K.A.M., and S.M.H.; Writing – original draft: D.L.S. and S.M.H.; Writing – review and editing: D.C.B., D.L.S., and S.M.H. All authors read the manuscript and provided comments. Funding acquisition: S.M.H.

Competing Interest Statement: The authors declare that they have no conflicts of interest with the contents of this article. The content is solely the responsibility of the authors and does not necessarily represent the official views of the National Institutes of Health.

578 **Figure Legends**

579

580 **Figure 1. The ufmylation activity of UFL1 promotes RIG-I signaling**.
581 A) IFN-β-promoter reporter luciferase expression (rel. to CMV-*Renilla*) from 293T cells
582 expressing vector, Flag-UFL1, or Flag-RIG-I, followed by mock or SenV infection (18 h).
583 B) RT-qPCR analysis (rel. to *18S*) of RNA extracted from primary neonatal human
584 dermal fibroblasts (NHDFs) transfected with either siCTRL or siUFL1 followed by mock
585 or SenV infection (8 h). C) ELISA for IFN-β of supernatants harvested from NHDFs
586 transfected with siCTRL or siUFL1 and infected with SenV for the indicated times. D)
587 Immunoblot analysis of p-IRF3 following siRNA transfection along with expression of
588 vector or Flag-UFL1^{siR}, which has point mutations in the siRNA seed sequence.
589 Quantification of p-IRF3/Tubulin is shown on underneath. E) Relative IFN-β-promoter
590 reporter luciferase expression (rel. to CMV-*Renilla*) from 293T cells expressing indicated
591 constructs followed by mock or SenV infection (12-18 h), with results graphed as relative
592 SenV fold change for each. For A) mean -/+ SD, n=3 technical replicates and
593 representative of n=3 independent experiments. For all others, mean -/+ SEM, n=3 or
594 n=5 (1E) biological replicates. *$p \leq 0.05$, **$p \leq 0.01$, and ***$p \leq 0.001$ determined by one-
595 way ANOVA followed by Šidák's multiple comparisons test (C), Student's t-test (B, D), or
596 one-way ANOVA followed by Dunnett's multiple comparisons test (E).

597

598 **Figure 2. The ufmylation machinery proteins positively regulate RIG-I signaling.**
599 A) IFN-β-promoter reporter luciferase expression (rel. to CMV-*Renilla*) from 293T cells
600 expressing vector, Flag-UFM1, or Flag-RIG-I followed by mock or SenV infection (18 h)
601 or in B) WT or CRISPR/CAS9 UFM1 KO 293T cells transfected with vector (Vec) or
602 Flag-UFM1 (for KO), followed by mock or SenV infection (18 h). C) ELISA for IFN-β of
603 supernatants harvested from WT or CRISPR/CAS9 UFM1 KO 293T cells that were
604 SenV infected (18 h). D) Diagram of UFM1 conjugation. E) Relative IFN-β-promoter
605 reporter luciferase expression (rel. to CMV-*Renilla*) from 293T cells expressing indicated
606 constructs followed by mock or SenV infection (18 h), with results graphed as relative
607 SenV fold change for each. F) RT-qPCR analysis (rel. to *GAPDH*) of RNA extracted from
608 293T WT, UFM1 KO or UFSP2 KO with either mock or SenV infection (18 h). For A)
609 mean -/+ SD, n=3 technical replicates and representative of n=3 independent
610 experiments. For all others, mean -/+ SEM, n=3 biological replicates. *$p \leq 0.05$, **$p \leq$
611 0.01, and ***$p \leq 0.001$ determined by two-way ANOVA followed by Tukey's multiple

612 comparisons test (A-B), Student's t-test (C), or one-way ANOVA followed by Dunnett's
613 multiple comparisons test (E, F).
614
615 **Figure 3. UFM1 is required for the RIG-I driven transcriptional response.**
616 RNA-seq analysis WT or UFM1 KO 293T cells following mock or SenV infection (18 h).
617 A) Gene set enrichment analysis of negatively regulated differentially expressed genes
618 in SenV-infected 293T cells represented by normalized enrichment score (UFM1 KO /
619 WT). B) Volcano plot of differentially expressed genes (adj P<0.01) shown in grey, with
620 ISGs shown in red, in SenV-infected 293T cells (UFM1 KO / WT). C) Heatmap of the
621 effect of UFM1 KO on the fold change of the 50 most induced IFN and ISGs (UFM1 KO /
622 WT) following SenV infection (adj P<0.01).
623
624 **Figure 4. UFL1 is recruited to intracellular membranes and interacts with 14-3-3ε**
625 **and RIG-I during RNA virus infection.**
626 A) Immunoblot analysis of inputs and subcellular membrane flotation of 293T cell
627 extracts that were mock or SenV-infected (4 h) followed by sucrose gradient
628 fractionation, with fraction numbers indicated from the top of the gradient (1) to bottom
629 (8). Fractionation controls, GAPDH for cytosol and Cox-I for membranes, are indicated
630 and reveal that the membranes are localized to fraction #1. Relative quantification of the
631 ratio of UFL1 to a membrane marker (Cox-I) in fraction 1 normalized to total protein
632 levels in inputs are shown on the right. B) Immunoblot analysis of anti-Flag
633 immunoprecipitated extracts and inputs from 293T cells expressing Myc-14-3-3ε and
634 Flag-UFL1 that were mock- or SenV-infected (4 h), with relative quantification on right.
635 C) Immunoblot analysis of anti-Flag immunoprecipitated extracts and inputs from 293T
636 cells expressing Myc-UFL1 and Flag-RIG-I that were mock- or SenV-infected (4 h), with
637 relative quantification with IP values normalized to inputs values on right. D) Immunoblot
638 analysis of anti-RIG-I immunoprecipitated (or anti-IgG) extracts and inputs from 293T
639 cells that were mock- or SenV-infected (4 h), with relative quantification with IP values
640 normalized to inputs values on right. E) Immunoblot analysis of anti-Flag
641 immunoprecipitated extracts and inputs from 293T cells expressing Myc-UFL1 and Flag-
642 RIG-I constructs that were mock- or SenV-infected (4 h), with results quantified as
643 relative fold change (SenV to Mock) for each. F) Relative IFN-β-promoter reporter
644 luciferase expression (rel. to CMV-*Renilla*) from 293T cells expressing indicated
645 constructs followed by mock or SenV infection (18 h), with results graphed as relative

646 SenV fold change for each. The graphs are represented as the mean -/+ SEM, n=3 (A-B,
647 D-F) or n=4 (C) biological replicates and *p ≤ 0.05, **p ≤ 0.01, and ***p ≤ 0.001
648 determined by Student's t-test (A-D) or one-way ANOVA followed by Dunnett's multiple
649 comparisons test (E-F).
650
651 **Figure 5. UFL1 interaction with RIG-I requires 14-3-3ε and ufmylation.**
652 A) Immunoblot analysis of anti-HA immunoprecipitated extracts and inputs from 293T
653 cells transfected with siCTRL or si14-3-3ε followed by SenV infection (4h). B)
654 Immunoblot of anti-HA immunoprecipitated extracts and inputs from 293T WT or UFM1
655 KO cells transfected with HA-RIG-I and Flag-UFL1. C) Immunoblot of anti-Flag
656 immunoprecipitated extracts and inputs from 293T WT or UFM1 KO cells transfected
657 with Flag-UFL1 and Myc-14-3-3ε. D) Immunoblot of anti-flag immunoprecipitated
658 extracts and inputs from either 293T-WT or 293T-Flag-14-3-3ε cells transfected with
659 either HA-UFM1-WT or HA-UFM1DC3. In (A-D), SenV infection was for 4 hours, and
660 relative quantification of the interacting protein vs. IP protein is shown underneath (A-C)
661 or as a graph (D), indicating the mean -/+ SEM (A, B, D), n=3 (A, B) or n=4 (D) biological
662 replicates. For (C) values shown are SD of IP values adjusted for input expression, with
663 n=2 biological replicates. *p ≤ 0.05, **p ≤ 0.01, and ***p ≤ 0.001 determined by Student's
664 t-test.
665
666 **Figure 6. Ufmylation promotes RIG-I interaction with 14-3-3ε for MAVS activation.**
667 A) Immunoblot of anti-Flag immunoprecipitated extracts and inputs from 293T cells
668 transfected with siCTRL or siUFL1 and indicated constructs. B) Immunoblot of anti-Myc
669 immunoprecipitated extracts from 293T WT or UFM1 KO cells. D) 293T WT or UFM1 KO
670 were mock or SenV-infected (12 h). Immunoblotting shows endogenous MAVS in input
671 samples and MAVS aggregation from P5 fractions, in the presence or absence of
672 denaturing reagent (β-mercaptoethanol). SenV infection was for 4 h (A-C) or 12 h (D). In
673 (A-B), relative quantification of interacting protein vs. IP protein in the IP is shown
674 underneath; in (D) SDD-AGE MAVS values are normalized to corresponding SDS-PAGE
675 values and shown as the ratio of SenV/mock values. Values (A-B) or graph (C) show the

676 mean -/+ SEM for n=3 biological replicates. *p ≤ 0.05, **p ≤ 0.01, and ***p ≤ 0.001
677 determined by Student's t-test.
678
679 **Figure S1. UFL1 positively regulates IFN induction.**
680 A) IFN-β-promoter reporter luciferase expression (rel. to CMV-*Renilla*) from 293T cells
681 transfected with vector (Vec) or Flag-UFL1, followed by mock or HCV PAMP RNA
682 transfection (24 h). B) RT-qPCR analysis (rel. to *GAPDH*) of RNA extracted from 293T
683 cells transfected vector or Flag-UFL1 that were treated with IFN-β (18 h). C) Quantification
684 of immunoblots from 293T cells expressing HA-UFM1, and either vector or indicated Flag-
685 UFL1 represented as the ratio of UFM1 conjugates (approximately 25-50 kDa) to total
686 protein expression in each lane with vector set to 100. Graph indicates the mean -/+ SEM
687 for n=3 biological replicates. *p ≤ 0.05 and **p ≤ 0.01 as determined by two-way ANOVA
688 followed by Šidák's multiple comparisons test (A), Student's t-test (B) or one-way ANOVA
689 followed by Dunnett's multiple comparisons test (C).
690
691 **Figure S2. Transcriptional response of genes negatively regulated by UFM1.**
692 RNA-seq analysis of WT versus UFM1 KO 293T cells showing the gene set enrichment
693 analysis (top 10 categories) of negatively regulated differentially expressed genes
694 represented by normalized enrichment score to identify gene ontology terms and
695 pathways associated with altered gene expression for each of the comparisons
696 performed (adj P<0.01).
697
698 **Figure S3. UFM1 is required for the interaction of RIG-I and 14-3-3ε.**
699 Immunoblot of anti-Flag immunoprecipitated extracts and inputs from 293T WT or UFM1
700 KO cells with relative quantification on the right. Graph shows the mean -/+ SEM for n=3
701 biological replicates; ***p ≤ 0.001 determined by Student's t-test.
702
703 **Dataset S1. Differential expression analysis from RNA-seq analysis for UFM1 KO /**
704 **WT 293T cells**
705 Table S1.1: UFM1 KO / WT Mock
706 Table S1.2 UFM1 KO / WT SenV (18 h)
707
708 **Dataset S2. Gene Set Enrichment Analysis for UFM1 KO / WT 293T cells**
709 Table S2.1: UFM1 KO / WT Mock- negative direction

710 Table S2.2 UFM1 KO / WT SenV (18 h)- negative direction

711 Table S2.3 UFM1 KO / WT Mock- positive direction

712 Table S2.4 UFM1 KO / WT SenV (18 h)- negative direction

713 **References**

714

715 1. D. Thoresen, *et al.*, The molecular mechanism of RIG-I activation and signaling.
716 *Immunol Rev* (2021) https:/doi.org/10.1111/imr.13022.

717 2. M. J. McFadden, N. S. Gokhale, S. M. Horner, Protect this house: cytosolic sensing
718 of viruses. *Current Opinion in Virology* **22**, 36–43 (2017).

719 3. J. Rehwinkel, M. U. Gack, RIG-I-like receptors: their regulation and roles in RNA
720 sensing. *Nature Reviews Immunology*, 1–15 (2020).

721 4. C. Chiang, M. U. Gack, Post-translational Control of Intracellular Pathogen Sensing
722 Pathways. *Trends in Immunology* **38**, 39–52 (2017).

723 5. M. U. Gack, *et al.*, TRIM25 RING-finger E3 ubiquitin ligase is essential for RIG-I-
724 mediated antiviral activity. *Nature* **446**, 916–920 (2007).

725 6. H. Oshiumi, M. Matsumoto, S. Hatakeyama, T. Seya, Riplet/RNF135, a RING
726 finger protein, ubiquitinates RIG-I to promote interferon-beta induction during the
727 early phase of viral infection. *J. Biol. Chem.* **284**, 807–817 (2009).

728 7. H. M. Liu, *et al.*, The Mitochondrial Targeting Chaperone 14-3-3ε Regulates a RIG-I
729 Translocon that Mediates Membrane Association and Innate Antiviral Immunity.
730 *Cell Host & Microbe* **11**, 528–537 (2012).

731 8. H. Oshiumi, Recent Advances and Contradictions in the Study of the Individual
732 Roles of Ubiquitin Ligases That Regulate RIG-I-Like Receptor-Mediated Antiviral
733 Innate Immune Responses. *Front Immunol* **11**, 1296 (2020).

734 9. Y. K. Chan, M. U. Gack, A phosphomimetic-based mechanism of dengue virus to
735 antagonize innate immunity. *Nature Immunology* **17**, 523–530 (2016).

736 10. W. Riedl, *et al.*, Zika Virus NS3 Mimics a Cellular 14-3-3-Binding Motif to
737 Antagonize RIG-I- and MDA5-Mediated Innate Immunity. *Cell Host & Microbe* **26**,
738 493-503.e6 (2019).

739 11. C. Vazquez, S. M. Horner, MAVS Coordination of Antiviral Innate Immunity. *J Virol*
740 **89**, 6974–6977 (2015).

741 12. E.-H. Tam, *et al.*, Role of the chaperone protein 14-3-3ε in the regulation of
742 influenza A virus-activated beta interferon. *J Virol*, JVI0023121 (2021).

743 13. S. M. Horner, H. M. Liu, H. S. Park, J. Briley, M. Gale, Mitochondrial-associated
744 endoplasmic reticulum membranes (MAM) form innate immune synapses and are
745 targeted by hepatitis C virus. *Proc Natl Acad Sci U S A* **108**, 14590–14595 (2011).

746 14. S. M. Horner, C. Wilkins, S. Badil, J. Iskarpatyoti, M. G. Jr, Proteomic Analysis of
747 Mitochondrial-Associated ER Membranes (MAM) during RNA Virus Infection

748 Reveals Dynamic Changes in Protein and Organelle Trafficking. *PLOS ONE* **10**,
749 e0117963 (2015).

750 15. D. C. Beachboard, *et al.*, The small GTPase RAB1B promotes antiviral innate
751 immunity by interacting with TNF receptor–associated factor 3 (TRAF3). *J. Biol.*
752 *Chem.*, jbc.RA119.007917 (2019).

753 16. K. Tatsumi, *et al.*, A novel type of E3 ligase for the Ufm1 conjugation system. *J.*
754 *Biol. Chem.* **285**, 5417–5427 (2010).

755 17. M. Komatsu, *et al.*, A novel protein-conjugating system for Ufm1, a ubiquitin-fold
756 modifier. *EMBO J* **23**, 1977–1986 (2004).

757 18. S. H. Kang, *et al.*, Two novel ubiquitin-fold modifier 1 (Ufm1)-specific proteases,
758 UfSP1 and UfSP2. *J. Biol. Chem.* **282**, 5256–5262 (2007).

759 19. Y. Wei, X. Xu, UFMylation: A Unique & Fashionable Modification for Life. *Genomics*
760 *Proteomics Bioinformatics* **14**, 140–146 (2016).

761 20. J. Daniel, E. Liebau, The Ufm1 Cascade. *Cells* **3**, 627–638 (2014).

762 21. L. Wang, *et al.*, UFMylation of RPL26 links translocation-associated quality control
763 to endoplasmic reticulum protein homeostasis. *Cell Res*, 1–16 (2019).

764 22. Z. Wang, *et al.*, MRE11 UFMylation promotes ATM activation. *Nucleic Acids*
765 *Research* **47**, 4124–4135 (2019).

766 23. H. M. Yoo, *et al.*, Modification of ASC1 by UFM1 is crucial for ERα transactivation
767 and breast cancer development. *Mol. Cell* **56**, 261–274 (2014).

768 24. B. Qin, *et al.*, UFL1 promotes histone H4 ufmylation and ATM activation. *Nat*
769 *Commun* **10**, 1242 (2019).

770 25. I. A. Gak, *et al.*, UFMylation regulates translational homeostasis and cell cycle
771 progression. *bioRxiv*, 2020.02.03.931196 (2020).

772 26. R. DeJesus, *et al.*, Functional CRISPR screening identifies the ufmylation pathway
773 as a regulator of SQSTM1/p62. *eLife* **5**, e17290 (2016).

774 27. J. R. Liang, *et al.*, A Genome-wide ER-phagy Screen Highlights Key Roles of
775 Mitochondrial Metabolism and ER-Resident UFMylation. *Cell* **0** (2020).

776 28. C. P. Walczak, *et al.*, Ribosomal protein RPL26 is the principal target of
777 UFMylation. *PNAS* **116**, 1299–1308 (2019).

778 29. Y. Cai, N. Singh, H. Li, Essential role of Ufm1 conjugation in the hematopoietic
779 system. *Exp. Hematol.* **44**, 442–446 (2016).

780 30. J. Kulsuptrakul, R. Wang, N. L. Meyers, M. Ott, A. S. Puschnik, A genome-wide
781 CRISPR screen identifies UFMylation and TRAMP-like complexes as host factors
782 required for hepatitis A virus infection. *Cell Reports* **34** (2021).

783 31. D. R. Balce, *et al.*, UFMylation inhibits the proinflammatory capacity of interferon-γ–
784 activated macrophages. *PNAS* **118** (2021).

785 32. Y.-M. Loo, *et al.*, Viral and therapeutic control of IFN-β promoter stimulator 1 during
786 hepatitis C virus infection. *PNAS* **103**, 6001–6006 (2006).

787 33. R. Sumpter, *et al.*, Regulating intracellular antiviral defense and permissiveness to
788 hepatitis C virus RNA replication through a cellular RNA helicase, RIG-I. *J Virol* **79**,
789 2689–2699 (2005).

790 34. T. Saito, D. M. Owen, F. Jiang, J. Marcotrigiano, M. Gale, Innate immunity induced
791 by composition-dependent RIG-I recognition of hepatitis C virus RNA. *Nature* **454**,
792 523–527 (2008).

793 35. D. Simsek, *et al.*, The Mammalian Ribo-interactome Reveals Ribosome Functional
794 Diversity and Heterogeneity. *Cell* **169**, 1051-1065.e18 (2017).

795 36. M. J. McFadden, *et al.*, Post-transcriptional regulation of antiviral gene expression
796 by N6-methyladenosine. *Cell Reports* **34**, 108798 (2021).

797 37. A. Peisley, B. Wu, H. Xu, Z. J. Chen, S. Hur, Structural basis for ubiquitin-mediated
798 antiviral signal activation by RIG-I. *Nature* **509**, 110–114 (2014).

799 38. A. Mizutani, M. Fukuda, K. Ibata, Y. Shiraishi, K. Mikoshiba, SYNCRIP, a
800 Cytoplasmic Counterpart of Heterogeneous Nuclear Ribonucleoprotein R, Interacts
801 with Ubiquitous Synaptotagmin Isoforms*. *Journal of Biological Chemistry* **275**,
802 9823–9831 (2000).

803 39. E. Foy, *et al.*, Control of antiviral defenses through hepatitis C virus disruption of
804 retinoic acid-inducible gene-I signaling. *Proc. Natl. Acad. Sci. U.S.A.* **102**, 2986–
805 2991 (2005).

806 40. E. Meylan, *et al.*, Cardif is an adaptor protein in the RIG-I antiviral pathway and is
807 targeted by hepatitis C virus. *Nature* **437**, 1167–1172 (2005).

808 41. X.-D. Li, L. Sun, R. B. Seth, G. Pineda, Z. J. Chen, Hepatitis C virus protease
809 NS3/4A cleaves mitochondrial antiviral signaling protein off the mitochondria to
810 evade innate immunity. *Proc Natl Acad Sci U S A* **102**, 17717–17722 (2005).

811 42. R. Lin, *et al.*, Dissociation of a MAVS/IPS-1/VISA/Cardif-IKKepsilon molecular
812 complex from the mitochondrial outer membrane by hepatitis C virus NS3-4A
813 proteolytic cleavage. *J Virol* **80**, 6072–6083 (2006).

814 43. K. Takahasi, *et al.*, Nonself RNA-Sensing Mechanism of RIG-I Helicase and
815 Activation of Antiviral Immune Responses. *Molecular Cell* **29**, 428–440 (2008).

816 44. H. Oshiumi, M. Miyashita, M. Matsumoto, T. Seya, A distinct role of Riplet-
817 mediated K63-Linked polyubiquitination of the RIG-I repressor domain in human
818 antiviral innate immune responses. *PLoS Pathog.* **9**, e1003533 (2013).

819 45. F. Hou, *et al.*, MAVS Forms Functional Prion-like Aggregates to Activate and
820 Propagate Antiviral Innate Immune Response. *Cell* **146**, 448–461 (2011).

821 46. N. Zamorano Cuervo, Q. Osseman, N. Grandvaux, Virus Infection Triggers MAVS
822 Polymers of Distinct Molecular Weight. *Viruses* **10** (2018).

823 47. W. Zeng, *et al.*, Reconstitution of the RIG-I pathway reveals a signaling role of
824 unanchored polyubiquitin chains in innate immunity. *Cell* **141**, 315–330 (2010).

825 48. X. Jiang, *et al.*, Ubiquitin-induced oligomerization of the RNA sensors RIG-I and
826 MDA5 activates antiviral innate immune response. *Immunity* **36**, 959–973 (2012).

827 49. L. Wang, *et al.*, UFMylation of RPL26 links translocation-associated quality control
828 to endoplasmic reticulum protein homeostasis. *Cell Research* **30**, 5–20 (2020).

829 50. Y. Zhang, M. Zhang, J. Wu, G. Lei, H. Li, Transcriptional regulation of the Ufm1
830 conjugation system in response to disturbance of the endoplasmic reticulum
831 homeostasis and inhibition of vesicle trafficking. *PLoS ONE* **7**, e48587 (2012).

832 51. C. Kwak, *et al.*, Contact-ID, a tool for profiling organelle contact sites, reveals
833 regulatory proteins of mitochondrial-associated membrane formation. *PNAS* **117**,
834 12109–12120 (2020).

835 52. Y. Merbl, P. Refour, H. Patel, M. Springer, M. W. Kirschner, Profiling of ubiquitin-
836 like modifications reveals features of mitotic control. *Cell* **152**, 1160–1172 (2013).

837 53. L. Wang, *et al.*, UFMylation of RPL26 links translocation-associated quality control
838 to endoplasmic reticulum protein homeostasis. *Cell Res.* **30**, 5–20 (2020).

839 54. M. Hochstrasser, Origin and function of ubiquitin-like proteins. *Nature* **458**, 422–
840 429 (2009).

841 55. K. N. Swatek, D. Komander, Ubiquitin modifications. *Cell Research* **26**, 399–422
842 (2016).

843 56. A. J. Muslin, J. W. Tanner, P. M. Allen, A. S. Shaw, Interaction of 14-3-3 with
844 Signaling Proteins Is Mediated by the Recognition of Phosphoserine. *Cell* **84**, 889–
845 897 (1996).

846 57. Y. Aghazadeh, V. Papadopoulos, The role of the 14-3-3 protein family in health,
847 disease, and drug development. *Drug Discovery Today* **21**, 278–287 (2016).

848 58. A. Aitken, Post-translational modification of 14-3-3 isoforms and regulation of
849 cellular function. *Seminars in Cell & Developmental Biology* **22**, 673–680 (2011).

850 59. J.-P. Lin, Y.-K. Fan, H. M. Liu, The 14-3-3η chaperone protein promotes antiviral
851 innate immunity via facilitating MDA5 oligomerization and intracellular
852 redistribution. *PLoS Pathog.* **15**, e1007582 (2019).

853 60. K. Onomoto, K. Onoguchi, M. Yoneyama, Regulation of RIG-I-like receptor-
854 mediated signaling: interaction between host and viral factors. *Cell Mol Immunol*
855 **18**, 539–555 (2021).

856 61. G. Liu, *et al.*, ISG15-dependent activation of the sensor MDA5 is antagonized by
857 the SARS-CoV-2 papain-like protease to evade host innate immunity. *Nature*
858 *Microbiology*, 1–12 (2021).

859 62. M. Yoneyama, *et al.*, Shared and Unique Functions of the DExD/H-Box Helicases
860 RIG-I, MDA5, and LGP2 in Antiviral Innate Immunity. *The Journal of Immunology*
861 **175**, 2851–2858 (2005).

862 63. C. Vazquez, C. Y. Tan, S. M. Horner, Hepatitis C Virus Infection Is Inhibited by a
863 Noncanonical Antiviral Signaling Pathway Targeted by NS3-NS4A. *Journal of*
864 *Virology* (2019) https:/doi.org/10.1128/JVI.00725-19 (February 8, 2022).

865 64. B. Fredericksen, *et al.*, Activation of the Interferon-β Promoter During Hepatitis C
866 Virus RNA Replication. *Viral Immunology* **15**, 29–40 (2002).

867 65. T. Saito, *et al.*, Regulation of innate antiviral defenses through a shared repressor
868 domain in RIG-I and LGP2. *PNAS* **104**, 582–587 (2007).

869 66. F. A. Ran, *et al.*, Genome engineering using the CRISPR-Cas9 system. *Nat Protoc*
870 **8**, 2281–2308 (2013).

871 67. Babraham Bioinformatics - Trim Galore! (October 12, 2021).

872 68. M. Martin, Cutadapt removes adapter sequences from high-throughput sequencing
873 reads. *EMBnet.journal* **17**, 10–12 (2011).

874 69. P. J. Kersey, *et al.*, Ensembl Genomes: an integrative resource for genome-scale
875 data from non-vertebrate species. *Nucleic Acids Res* **40**, D91-97 (2012).

876 70. A. Dobin, *et al.*, STAR: ultrafast universal RNA-seq aligner. *Bioinformatics* **29**, 15–
877 21 (2013).

878 71. HTSeq: Analysing high-throughput sequencing data with Python — HTSeq 0.13.5
879 documentation (October 12, 2021).

880 72. M. I. Love, W. Huber, S. Anders, Moderated estimation of fold change and
881 dispersion for RNA-seq data with DESeq2. *Genome Biology* **15**, 550 (2014).

882 73. W. Huber, *et al.*, Orchestrating high-throughput genomic analysis with
883 Bioconductor. *Nat Methods* **12**, 115–121 (2015).

884 74. V. K. Mootha, *et al.*, PGC-1alpha-responsive genes involved in oxidative
885 phosphorylation are coordinately downregulated in human diabetes. *Nat Genet* **34**,
886 267–273 (2003).

887 75. H. M. Liu, *et al.*, SYNCRIP (synaptotagmin-binding, cytoplasmic RNA-interacting
888 protein) is a host factor involved in hepatitis C virus RNA replication. *Virology* **386**,
889 249–256 (2009).

890

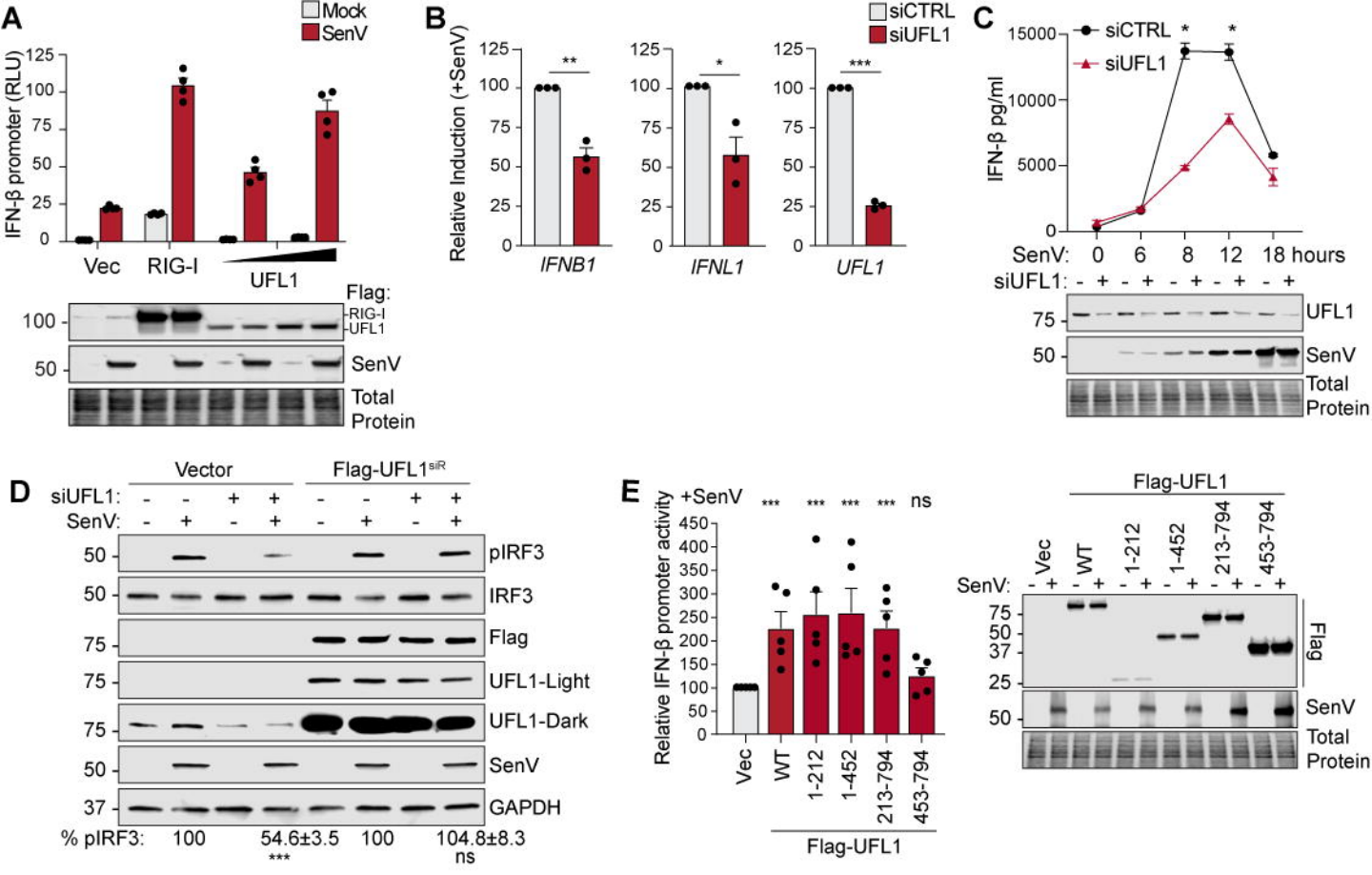
A
Mock
SenV
IFN-β promoter (RLU)
125
100
75
50
25
0
Vec
RIG-I
UFL1
Flag:
RIG-I
UFL1
100
50
SenV
Total Protein
B
siCTRL
siUFL1
Relative Induction (+SenV)
125
100
75
50
25
0
**
*
***
IFNB1
IFNL1
UFL1
C
siCTRL
siUFL1
IFN-β pg/ml
15000
10000
5000
0
*
*
SenV: 0 6 8 12 18 hours
siUFL1: - + - + - + - + - +
75
50
UFL1
SenV
Total Protein
D
Vector
Flag-UFL1siR
siUFL1: - - + + - - + +
SenV: - + - + - + - +
50
pIRF3
50
IRF3
75
Flag
75
UFL1-Light
75
UFL1-Dark
50
SenV
37
GAPDH
% pIRF3: 100 54.6±3.5 100 104.8±8.3
***
ns
E
+SenV
Relative IFN-β promoter activity
450
400
350
300
250
200
150
100
50
0
***
***
***
***
ns
Vec
WT
1-212
1-452
213-794
453-794
Flag-UFL1
Flag-UFL1
Vec
WT
1-212
1-452
213-794
453-794
SenV: - + - + - + - + - + - +
75
50
37
25
Flag
50
SenV
Total Protein

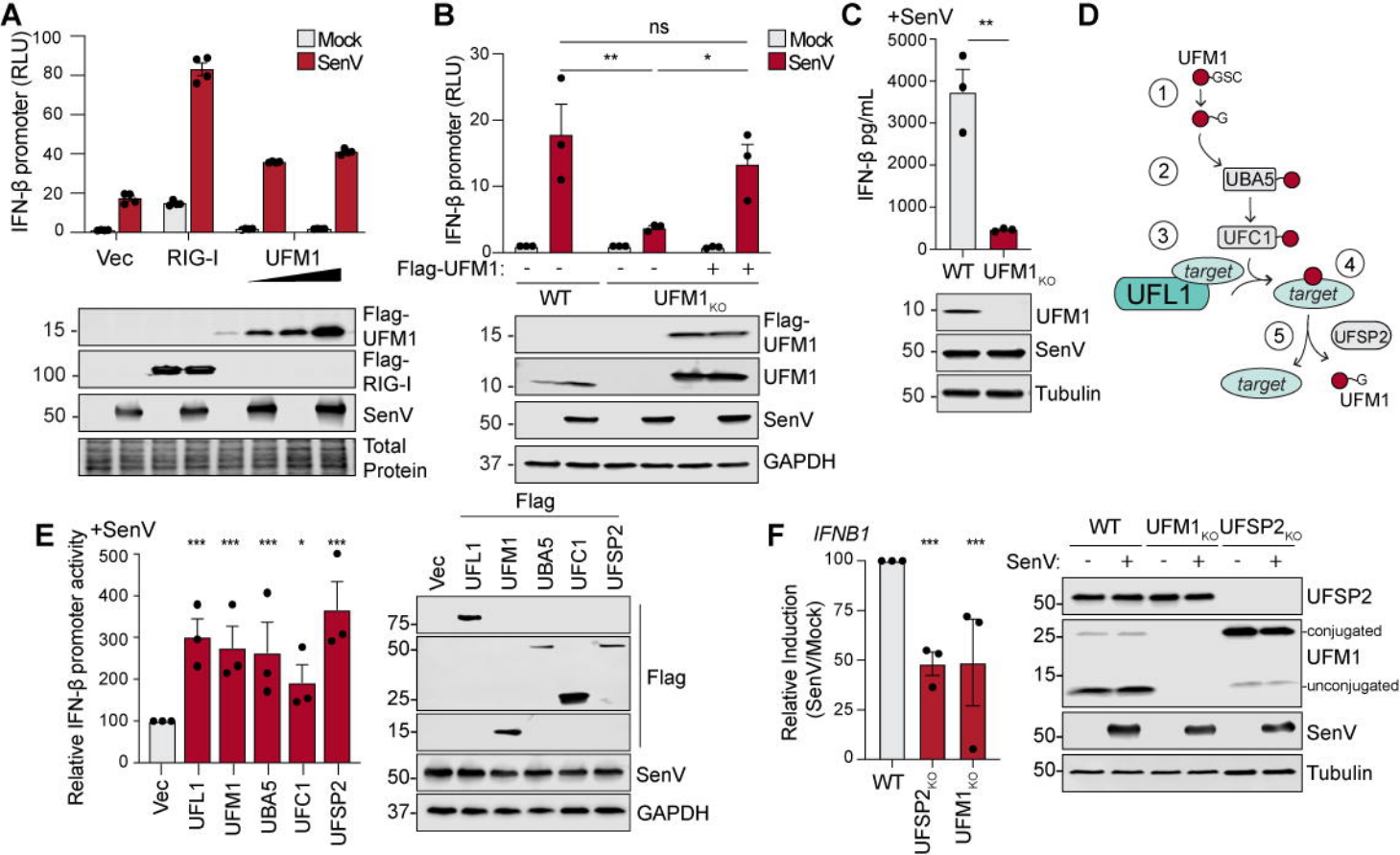
A
IFN-β promoter (RLU)
Mock
SenV
Vec
RIG-I
UFM1
Flag-UFM1
Flag-RIG-I
SenV
Total Protein
B
ns
**
*
IFN-β promoter (RLU)
Mock
SenV
Flag-UFM1:
WT
UFM1KO
Flag-UFM1
UFM1
SenV
GAPDH
C
+SenV
**
IFN-β pg/mL
WT
UFM1KO
UFM1
SenV
Tubulin
D
UFM1
GSC
G
UBA5
UFC1
UFL1
target
UFSP2
E
+SenV
Relative IFN-β promoter activity
Vec
UFL1
UFM1
UBA5
UFC1
UFSP2
Flag
SenV
GAPDH
F
IFNB1
Relative Induction (SenV/Mock)
WT
UFSP2KO
UFM1KO
SenV:
UFSP2
conjugated
UFM1
unconjugated
SenV
Tubulin

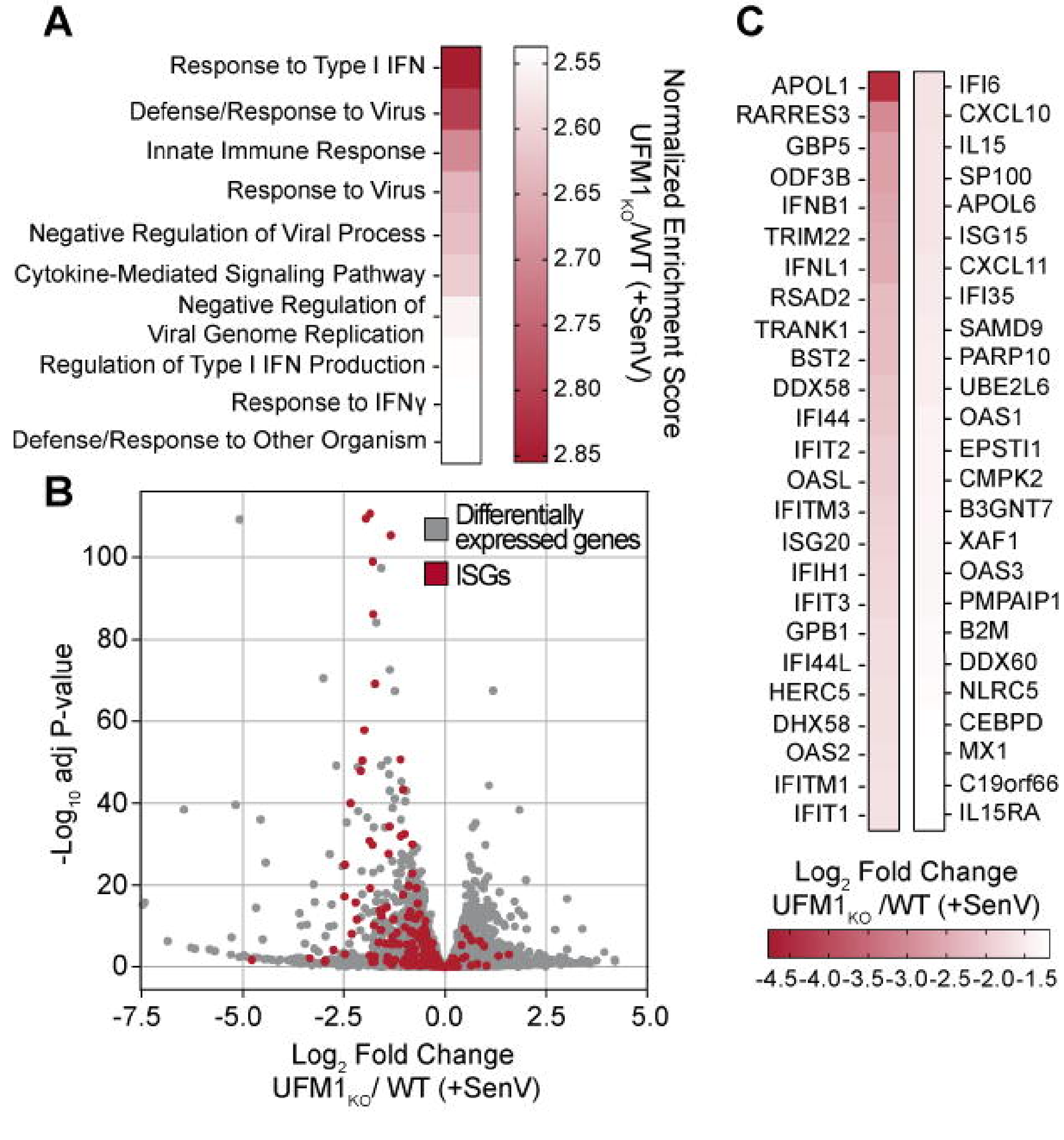
A
Response to Type I IFN
Defense/Response to Virus
Innate Immune Response
Response to Virus
Negative Regulation of Viral Process
Cytokine-Mediated Signaling Pathway
Negative Regulation of Viral Genome Replication
Regulation of Type I IFN Production
Response to IFNγ
Defense/Response to Other Organism
2.55
2.60
2.65
2.70
2.75
2.80
2.85
Normalized Enrichment Score
UFM1KO/WT (+SenV)
B
Differentially expressed genes
ISGs
-Log10 adj P-value
100
80
60
40
20
0
-7.5
-5.0
-2.5
0.0
2.5
5.0
Log2 Fold Change
UFM1KO/ WT (+SenV)
C
APOL1
RARRES3
GBP5
ODF3B
IFNB1
TRIM22
IFNL1
RSAD2
TRANK1
BST2
DDX58
IFI44
IFIT2
OASL
IFITM3
ISG20
IFIH1
IFIT3
GPB1
IFI44L
HERC5
DHX58
OAS2
IFITM1
IFIT1
IFI6
CXCL10
IL15
SP100
APOL6
ISG15
CXCL11
IFI35
SAMD9
PARP10
UBE2L6
OAS1
EPSTI1
CMPK2
B3GNT7
XAF1
OAS3
PMPAIP1
B2M
DDX60
NLRC5
CEBPD
MX1
C19orf66
IL15RA
Log2 Fold Change
UFM1KO /WT (+SenV)
-4.5-4.0-3.5-3.0-2.5-2.0-1.5

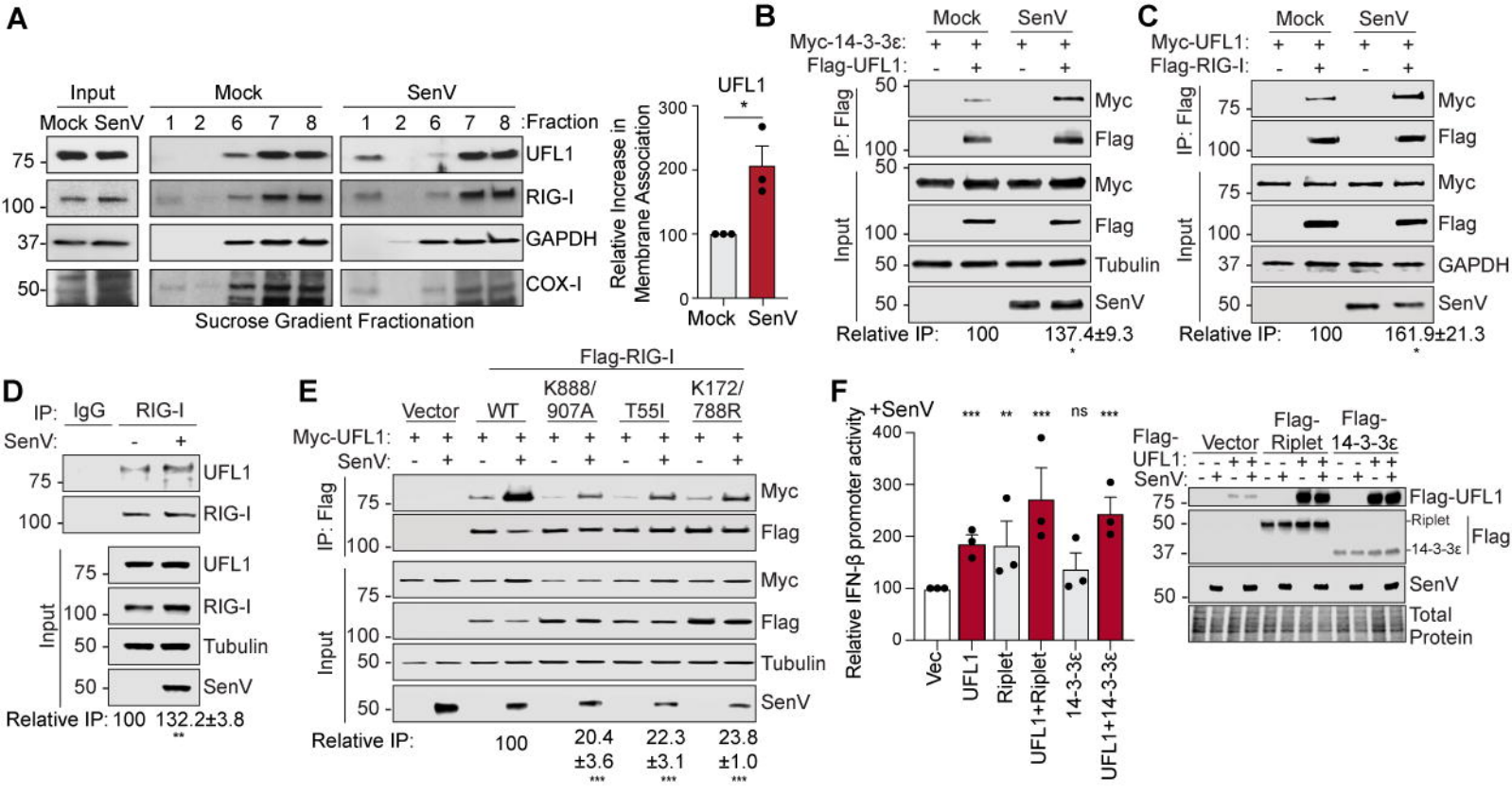
A
Input
Mock SenV
Mock
1 2 6 7 8
SenV
1 2 6 7 8 :Fraction
75
100
37
50
UFL1
RIG-I
GAPDH
COX-I
Sucrose Gradient Fractionation
UFL1
Relative Increase in Membrane Association
300
200
100
0
Mock SenV
B
Mock SenV
Myc-14-3-3ε:
Flag-UFL1:
IP: Flag
Input
Myc
Flag
Tubulin
SenV
Relative IP: 100 137.4±9.3
C
Mock SenV
Myc-UFL1:
Flag-RIG-I:
IP: Flag
Input
Myc
Flag
GAPDH
SenV
Relative IP: 100 161.9±21.3
D
IP: IgG RIG-I
SenV: - +
UFL1
RIG-I
Input
Tubulin
SenV
Relative IP: 100 132.2±3.8
E
Flag-RIG-I
Vector WT K888/907A T55I K172/788R
Myc-UFL1:
SenV:
IP: Flag
Input
Myc
Flag
Tubulin
SenV
Relative IP: 100 20.4 ±3.6 22.3 ±3.1 23.8 ±1.0
F
+SenV
Relative IFN-β promoter activity
400
300
200
100
0
Vec UFL1 Riplet UFL1+Riplet 14-3-3ε UFL1+14-3-3ε
Flag-UFL1
Riplet
14-3-3ε
Flag
SenV
Total Protein

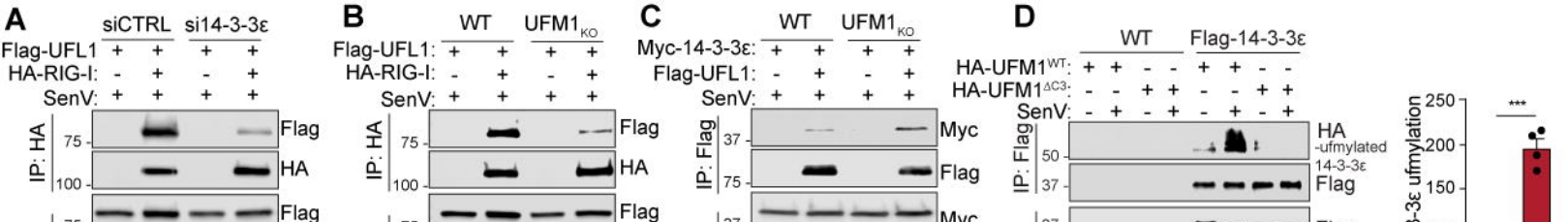
A
siCTRL
si14-3-3ε
Flag-UFL1
HA-RIG-I:
SenV:
IP: HA
Input
Flag
HA
14-3-3ε
SenV
Tubulin
Relative IP: 100 15.6±4.3
***
B
WT
UFM1KO
Flag-UFL1:
HA-RIG-I:
SenV:
IP: HA
Input
Flag
HA
UFM1
SenV
Tubulin
Relative IP: 100 62.7±13.2
*
C
WT
UFM1KO
Myc-14-3-3ε:
Flag-UFL1:
SenV:
IP: Flag
Input
Myc
Flag
UFM1
SenV
Tubulin
Relative IP: 100 120.1±6.1
D
WT
Flag-14-3-3ε
HA-UFM1WT:
HA-UFM1ΔC3:
SenV:
IP: Flag
Input
HA -ufmylated
14-3-3ε
Flag
HA
SenV
Tubulin
Relative 14-3-3ε ufmylation
***
Mock
SenV

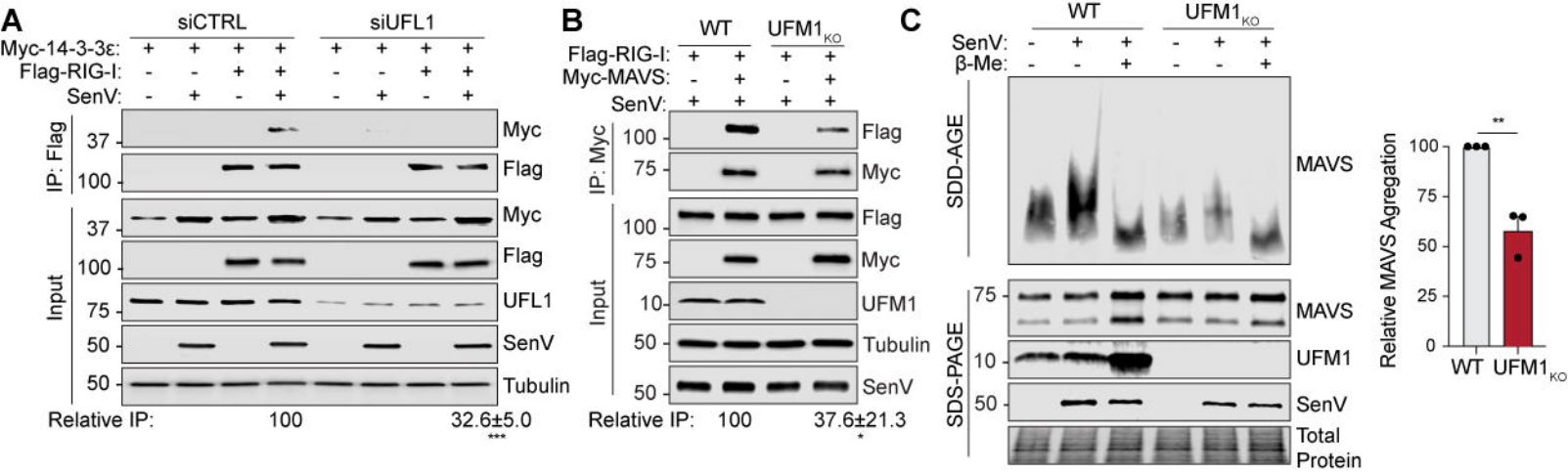
A
siCTRL
siUFL1
Myc-14-3-3ε:
Flag-RIG-I:
SenV:
IP: Flag
Input
Myc
Flag
UFL1
SenV
Tubulin
Relative IP:
100
32.6±5.0
***
B
WT
UFM1KO
Flag-RIG-I:
Myc-MAVS:
SenV:
IP: Myc
Input
Flag
Myc
UFM1
Tubulin
SenV
Relative IP:
100
37.6±21.3
*
C
WT
UFM1KO
SenV:
β-Me:
SDD-AGE
SDS-PAGE
MAVS
UFM1
SenV
Total Protein
Relative MAVS Agregation
**
WT
UFM1KO

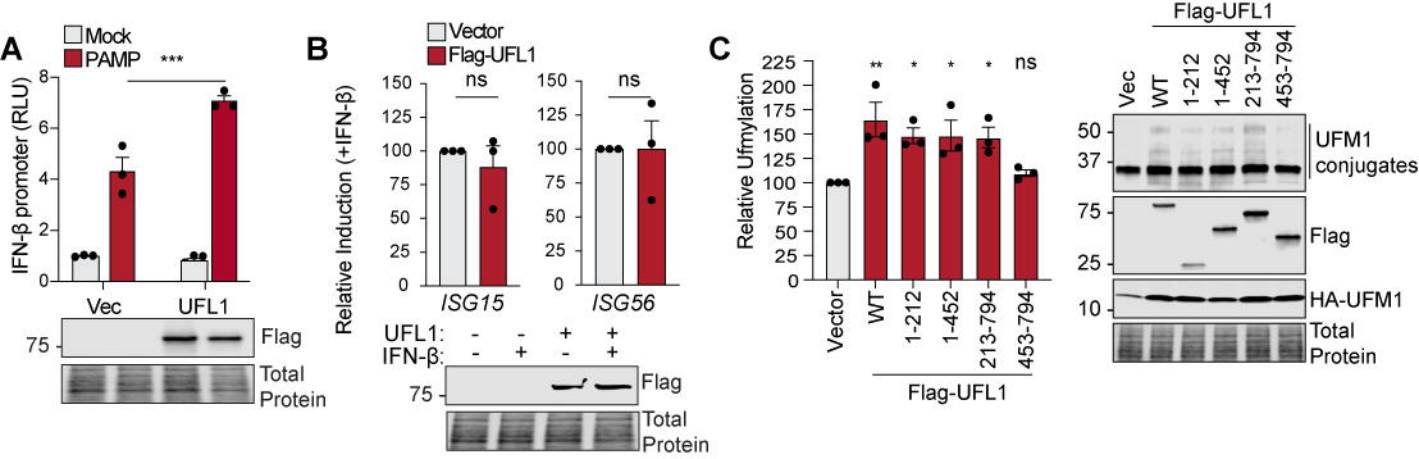
A
Mock
PAMP
***
IFN-β promoter (RLU)
8
6
4
2
0
Vec
UFL1
75
Flag
Total Protein
B
Vector
Flag-UFL1
Relative Induction (+IFN-β)
150
125
100
75
50
25
0
ns
ns
ISG15
ISG56
UFL1: - - + +
IFN-β: - + - +
75
Flag
Total Protein
C
Relative Ufmylation
225
200
175
150
125
100
75
50
25
0
**
*
*
*
ns
Vector
WT
1-212
1-452
213-794
453-794
Flag-UFL1
Flag-UFL1
Vec
WT
1-212
1-452
213-794
453-794
50
37
UFM1 conjugates
75
25
Flag
10
HA-UFM1
Total Protein

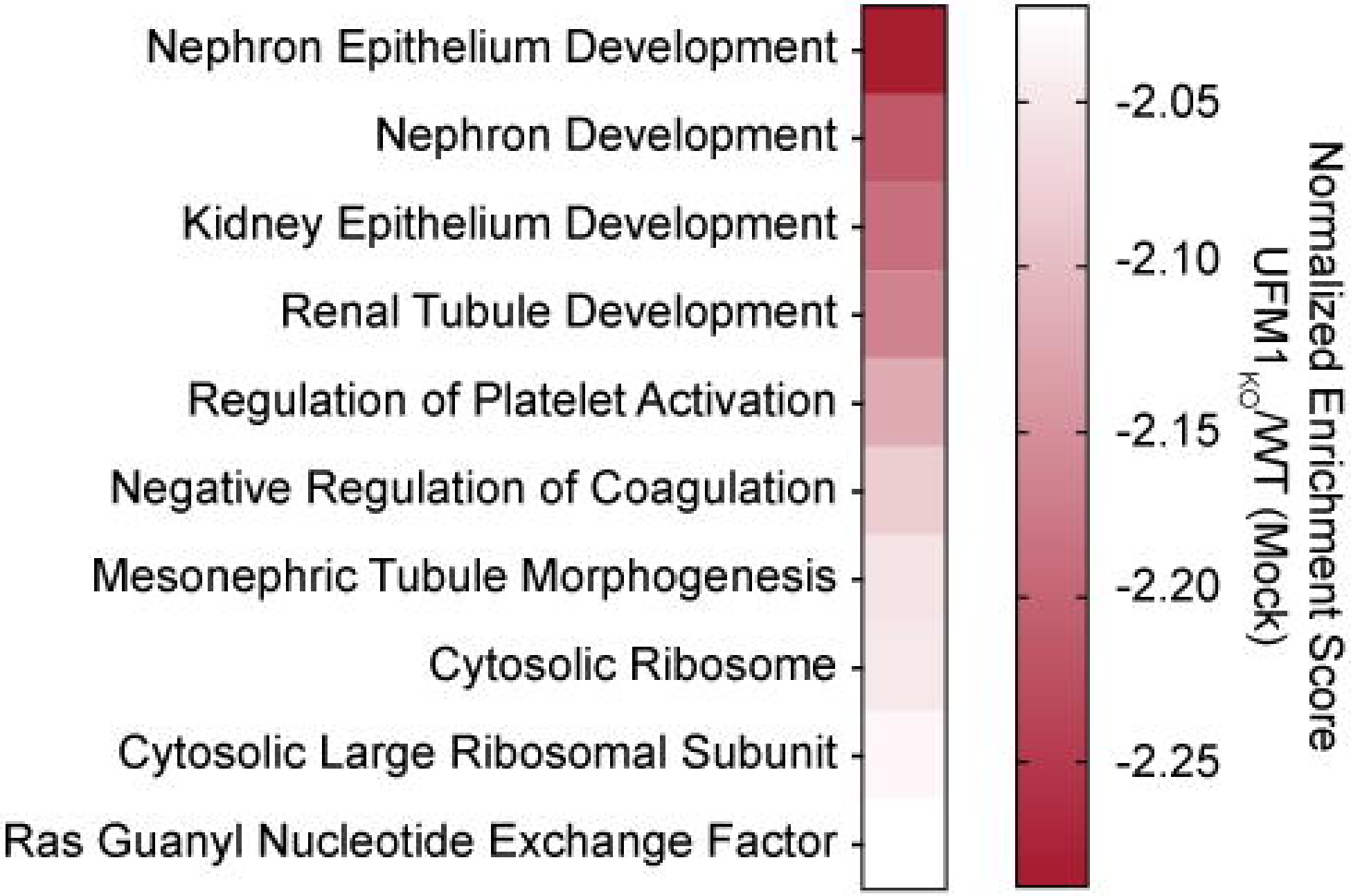
Nephron Epithelium Development
Nephron Development
Kidney Epithelium Development
Renal Tubule Development
Regulation of Platelet Activation
Negative Regulation of Coagulation
Mesonephric Tubule Morphogenesis
Cytosolic Ribosome
Cytosolic Large Ribosomal Subunit
Ras Guanyl Nucleotide Exchange Factor
-2.05
-2.10
-2.15
-2.20
-2.25
Normalized Enrichment Score
UFM1KO/WT (Mock)

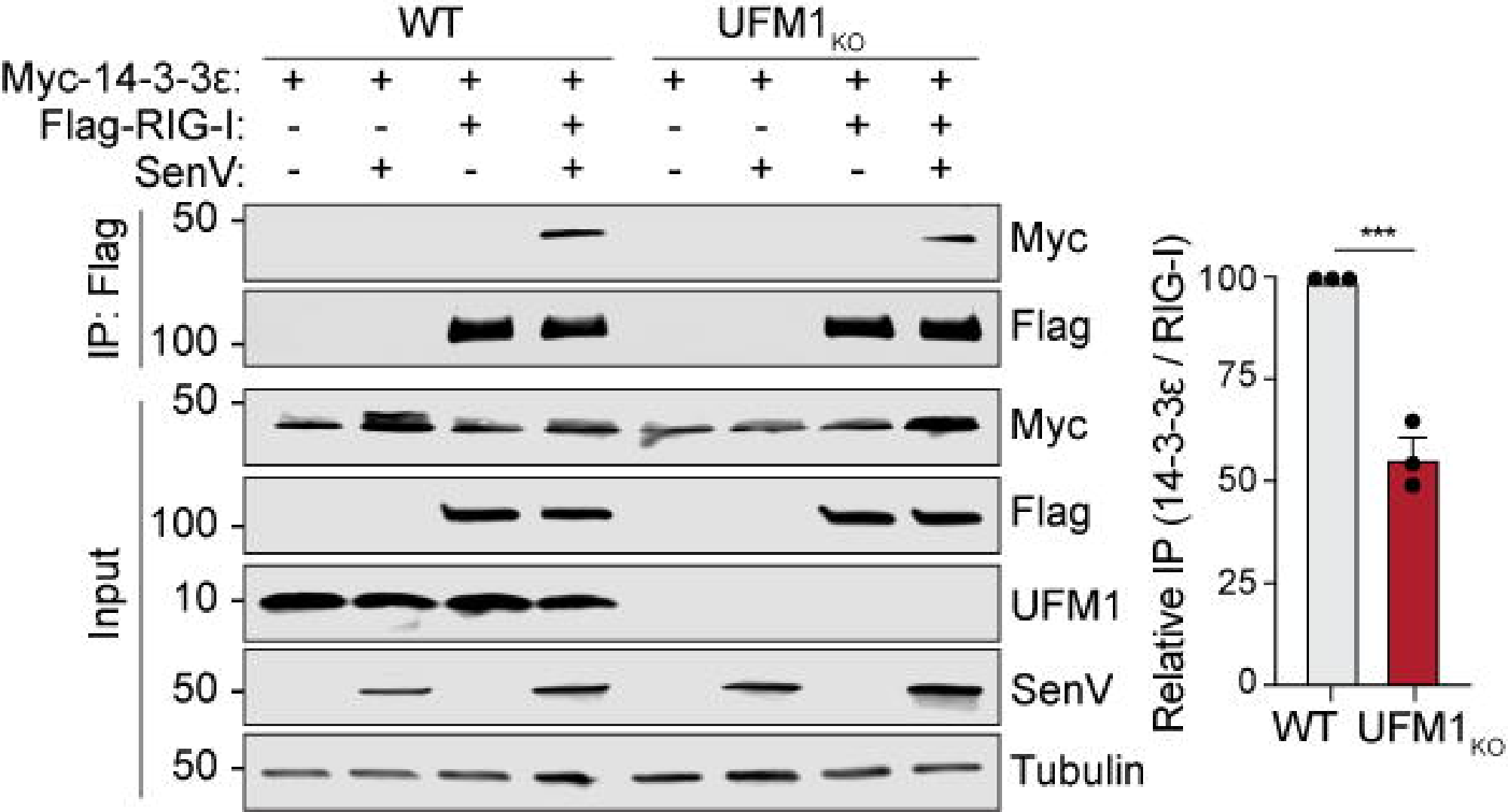
WT
UFM1KO
Myc-14-3-3ε:
Flag-RIG-I:
SenV:
IP: Flag
Input
50
100
10
Myc
Flag
UFM1
SenV
Tubulin
Relative IP (14-3-3ε / RIG-I)
***
100
75
50
25
0
WT
UFM1KO